

2011

# Investigation of ply waviness in wind turbine blades: Experimental and numerical analysis

Sunil Kishore Chakrapani  
*Iowa State University*

Follow this and additional works at: <https://lib.dr.iastate.edu/etd>

 Part of the [Aerospace Engineering Commons](#)

## Recommended Citation

Chakrapani, Sunil Kishore, "Investigation of ply waviness in wind turbine blades: Experimental and numerical analysis" (2011).  
*Graduate Theses and Dissertations*. 10175.  
<https://lib.dr.iastate.edu/etd/10175>

This Thesis is brought to you for free and open access by the Iowa State University Capstones, Theses and Dissertations at Iowa State University Digital Repository. It has been accepted for inclusion in Graduate Theses and Dissertations by an authorized administrator of Iowa State University Digital Repository. For more information, please contact [digirep@iastate.edu](mailto:digirep@iastate.edu).

**Investigation of ply waviness in wind turbine blades: Experimental and numerical analysis**

By

**Sunil Kishore Chakrapani**

A thesis submitted to the graduate faculty  
in partial fulfillment of the requirements for the degree of  
**MASTER OF SCIENCE**

Major: Engineering Mechanics

Program of Study Committee:  
Vinay Dayal, Major Professor  
David K. Hsu  
Matthew C. Frank  
Dan J. Barnard

Iowa State University

Ames, Iowa

2011

Copyright © Sunil Kishore Chakrapani, 2011. All rights reserved.

## TABLE OF CONTENTS

LIST OF FIGURES .....	iv
LIST OF TABLES .....	vii
ABSTRACT .....	viii
CHAPTER 1. INTRODUCTION.....	1
1.1 PROBLEM DEFINITION.....	1
1.2 OBJECTIVE.....	3
1.3 THESIS ORGAINIZATION.....	4
CHAPTER 2.ULTRASONIC RAYLEIGH WAVE INSPECTION OF WAVINESS IN WIND TURBINE BLADES: EXPERIMENTAL AND FINITE ELEMENT METHOD.....	5
1. INTRODUCTION.....	6
2. PROBLEM STATEMENT .....	8
3. BACKGROUND.....	9
4. SAMPLES USED.....	15
5. EXPERIMENTAL SETUP .....	17
5.1. LABORATORY BASED SYSTEM.....	17
5.2. STANDALONE SYSTEM .....	18
6. RESULTS.....	22
6.1. DETECTION - Part A.....	22
6.2. DETECTION – Part B.....	23
6.3. CHARACTERIZATION.....	29
6.4. CHARACTERIZATION DISCUSSIONS .....	29
7. FINITE ELEMENT MODELING .....	35
7.1. NUMERICAL B SCAN.....	37
8. DISCUSSIONS .....	44
9. CONCLUSION .....	48
CHAPTER 3. BOND THICKNESS MEASURMENT.....	49
3.1. METHOD AND THEORY .....	50
3.2 EXPERIMENTAL SETUP .....	53
3.3 RESULTS.....	53

3.4 DISCUSSIONS .....	54
CHAPTER 4. CONCLUSIONS.....	54
4.1 SUMMARY .....	54
4.2 FUTURE WORK .....	55
REFERENCES.....	56

## LIST OF FIGURES

### CHAPTER 1

**Fig 1.1:** Detailed section of wind turbine blade showing the three major structural members; spar cap, trailing edge and leading edge [17]. 3

### CHAPTER 2:

**Fig. 1:** Definition of aspect ratio of a discrete marcel 8

**Fig.2:** Axis rotation of angled laminate 10

**Fig.3:** Variation of bulk wave speed (longitudinal and shear) with fiber deviation angle 19

**Fig.4:** Schematic of the Laboratory based scanning system used as a proof-of-concept tool. 20

**Fig.5:** Schematic of the standalone scanning system. 20

**Fig.6:** 8x micrograph of discrete out of plane marcel of AR 14 21

**Fig.7:** 8x micrograph of discrete out of plane marcel of AR 10 21

**Fig. 8:** Schematic of experimental setup. Wave propagation direction is parallel to the direction of marcel and perpendicular to the direction of unidirectional fibers. 25

**Fig. 9:** C-Scan marcel of AR 8, (a) Downward pointing marcel, (b) Upward pointing marcel 25

**Fig.10:** C-Scan results of standard samples using laboratory based system for (a) WS-01, (b) WS-02, (c) WS-03, (d) WS-04, (e) WS-05, and (f) WS-06. The detected marcel are marked with a white circle. 26, 27, 28

<b>Fig.11:</b> C-Scan results of trailing edge samples, (a) Wave H, I (b) Wave K, L (c) Wave I, J (d) Wave M, N	32
<b>Fig.12:</b> Damage index vs. Aspect ratio for marcel at 6, 12 and 18mm depth. Information from Table 2-6 was used to plot this.	33
<b>Fig.13:</b> High resolution B scans using 2.25 MHz contact transducers. (a) Wave H, L (b) Wave J, N (c) Wave I, M	33, 34
<b>Fig.14:</b> 2-D ANSYS model of discrete, out-of-plane waviness	35
<b>Fig.15:</b> Numerical A-Scan of Rayleigh wave.	37
<b>Fig.16:</b> Numerical B-Scan of marcel AR6 at 100 KHz, and placed at 6mm	38
<b>Fig.17:</b> Numerical B-Scan of marcel AR6 at 200 KHz, at 6mm	38
<b>Fig.18:</b> Numerical B-Scan of marcel AR6, at 12mm	39
<b>Fig.19:</b> Numerical B-Scan of marcel AR6 at 18mm	39
<b>Fig.20:</b> Hilbert transform of B-Scan for marcel at 6mm (Shown in Fig.16)	40
<b>Fig.21:</b> Hilbert transform of B-Scan for marcel at 12mm (Shown in Fig.17)	41
<b>Fig.22:</b> Hilbert transform of B-Scan for marcel at 18mm (Shown in Fig.18)	41
<b>Fig.23:</b> A-Scan of 0.7mm ply laminate (40 layers). The primary and secondary modes are shown.	43
<b>Fig.24:</b> A-Scan of 0.3mm plies laminate (40 layers). Notice the secondary mode travelling faster than the secondary mode of 0.7mm ply.	43
<b>Fig.25:</b> The measurement plane in the XY plane of the marcel.	45
<b>Fig. 26:</b> Out of plane stress (Y) distribution for downward pointing marcel (AR 6) across the thickness at the center of marcel.	46

- Fig.27:** Out of plane stress (Y) distribution for upward pointing marcel (AR 6) across the thickness at the center of marcel. 46
- Fig.28:** Shear Stress (XY) distribution for downward pointing marcel (AR 6) across the thickness at the center of marcel. 47
- Fig.29:** Shear Stress (XY) distribution for upward pointing marcel (AR 6) across the thickness at the center of marcel. 47

### CHAPTER 3

- Fig. 3.1:** Section of the bond joint between the two halves of the blade. 49
- Fig. 3.2:** Schematic of shear web/spar cap joint bond-line. 50
- Fig.3.3:** Schematic of pulse echo method used for inspection. 51
- Fig.3.4:** The adhesive and spar cap signal in time domain. 52
- Fig.3.5:** schematic of bond-line measurement setup 52

## LIST OF TABLES

### CHAPTER 2

<b>TABLE I:</b> List of Samples used for experiments and their details	16
<b>TABLE.II:</b> Summary of upward and downward pointing marcel characteristics.	25
<b>TABLE.III:</b> B Scan of WS-01	31
<b>TABLE.IV:</b> B Scan of WS-02	31
<b>TABLE.V:</b> B Scan of WS-03	31
<b>TABLE.VI:</b> B Scan of WS-04	31
<b>TABLE.VII:</b> B Scan of WS-05	31
<b>TABLE.VIII:</b> Material properties of laminate and epoxy used for numerical modeling.	36



## ABSTRACT

Composite materials used in fabricating wind turbine blades use large tows, stitched fibers which are relatively thick compared to the composites used in many other applications. Thick fibers enables manufactures to save cost of the fiber and build up the thickness quickly, but introduces defects such as waviness, dry patch etc. Waviness in composites has been shown to degrade the tensile and compressive strength of the laminate. Waviness in a critical portion of the blade can lead to the catastrophic failure of the blade which is costly not only from the cost of the equipment but also the loss of power generation.

This thesis presents the results of investigation of intrinsic, discrete, and out of plane waviness in wind turbine blades using non-destructive evaluation. A field implementable, Rayleigh wave based scanning system using air coupled transducers was devised and tested. Further the detected discrete waves (marcels) were characterized in terms of aspect ratio which is a non-dimensional characteristic of the marcel. This kind of system enables manufactures to detect and quantify defects, to determine if it really poses a threat to the structural integrity of the blade. To understand the mechanics better, finite element analysis of wave propagation in wavy laminates was performed and compared to experimental results.

Another area of interest in a blade is the bond joint between spar cap and shear web. This work was undertaken and the bond thickness was measured using contact ultrasonics NDE. Using the initial results a field implementable system was developed and was used for field tests.

## CHAPTER 1. INTRODUCTION

### 1.1 PROBLEM DEFINITION

Wind turbine is an electro-mechanical device used to convert kinetic wind energy into mechanical energy, which is in-turn used to convert into electrical energy with the help of generators. Wind turbines have been known to be used as early as 600 B.C in Persia for digging water and in China for grinding seeds. The simple design of the wind turbine makes it easy to manufacture and its ability to convert wind into usable power, makes it a quasi-perpetual machine in modern terms. Over the years of human evolution, the blade design has remained the same. To increase the efficiency of the system, wind turbines were scaled up in size, positioned off-shore to extract higher winds, etc. The widely used 1.5 MW wind turbines by Suzlon® and Clipper® are slowly paving its way for 2.5 MW systems. Built upon its predecessor's base design, the 2.5 MW blades are bigger and more efficient than the 1.5 MW turbines. But since the turbine blades are much bigger, the blade mass scales as a cube of the turbine radius. This leads to the use of lighter yet stronger materials. Although aluminum has been used previously for making wind turbine blades, contemporarily, Fiber glass composite has been used widely to save weight and increases the structural integrity. With the use of any new materials, one has to be prepared for new challenges like defects such as delamination, waviness, dry fibers, and ply drop-offs etc. which do not exist in the case of conventional materials like aluminum and steel.

This research concentrates on detecting and characterizing such defects found in composite wind turbine blades. In specific, defects such as waviness and bonded joints have been studied. For this study, composite sections with engineered defects were fabricated in-house, and nondestructive testing was used to test and evaluate defects. NDE has a wide spectrum of methods under it, but ultrasonics was used in this study, due to its easy field adaptability, and needlessness of skilled labor. Current NDE methods used include visual inspection, high intensity light inspection, contact ultrasonics and thermography. A very important goal of this work was field adaptability and we succeeded in building a system which will be shown in later sections.

The composite wind turbine blade consists of three vital structural members, and they are: spar cap, trailing edge, and leading edge. Figure (1.1) shows the construction of a typical wind turbine blade. The blade is mostly made of glass fibers, and the three members encounter maximum stress under loading conditions. Hence a failure in one of these structures will result in the catastrophic failure of the entire blade. A very stringent quality control in these structures is desired, which is addressed in this study.

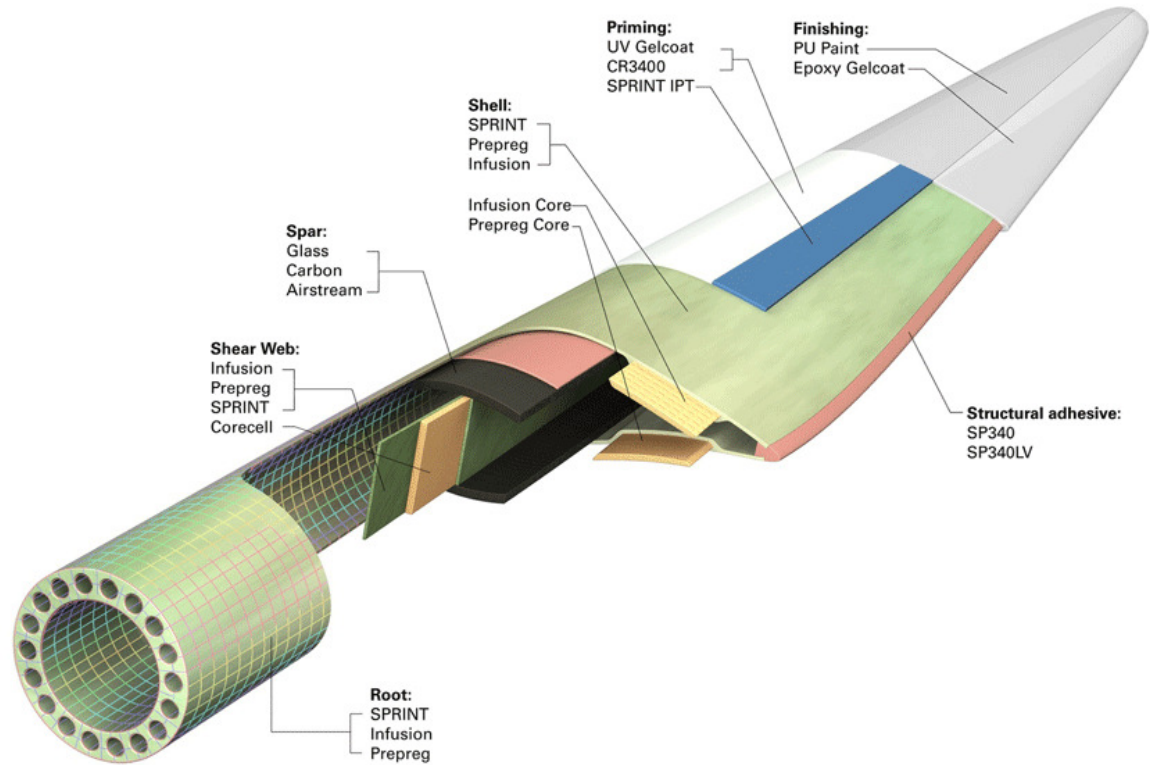


**Fig 1.1:** Detailed section of wind turbine blade showing the three major structural members; spar cap, trailing edge and leading edge [17].

## 1.2 OBJECTIVE

The objective of this research is to study the effect of defects found in composite wind turbine blades using ultrasonic Non-destructive evaluation. A field implementable system has to be designed with the inputs from the study, and later used to test and evaluate the corresponding defects. This thesis is limited to the study of waviness in composite sections and measurement of adhesive thickness in wind turbine blades. Furthermore, only intrinsic, discrete, out-of-plane waviness has been studied and reported.

### 1.3 THESIS ORGANIZATION

In Chapter 2, the work done on waviness including the theoretical background behind waviness in terms of material behavior, non-destructive testing results and the use of finite element method to understand the mechanics of wave propagation in wavy laminate has been presented.

Chapter 3 highlights the current work in terms of bond-line measurement in composite wind turbine blades. The use of low frequency contact ultrasonic transducers to determine the bond-line thickness has been described in detail.

Chapter 4 wraps this thesis with a summary of work, general discussions and conclusions based on the research. Future work is identified and reported in this chapter.

## CHAPTER 2. ULTRASONIC RAYLEIGH WAVE INSPECTION OF WAVINESS IN WIND TURBINE BLADES: EXPERIMENTAL AND FINITE ELEMENT METHOD

A paper to be submitted to *NDT & E, Elsevier*.

**Sunil Kishore Chakrapani**

Center for Nondestructive Evaluation, Department of  
Aerospace Engineering, Iowa State University  
Ames, Iowa, USA 50010

**Vinay Dayal**

Center for Nondestructive Evaluation, Department of  
Aerospace Engineering, Iowa State University  
Ames, Iowa, USA 50010

**Daniel Barnard**

Center for Nondestructive  
Evaluation, Iowa State University  
Ames, Iowa, USA 50010

**David Hsu**

Center for Nondestructive  
Evaluation, Iowa State University  
Ames, Iowa, USA 50010

### ABSTRACT

With the need for larger and more efficient wind turbine blades, thicker composite sections are manufactured and waviness becomes difficult to control. Thus, there is a need for more effective and field implementable NDE. In this paper we propose a method of detection and quantification of waviness in composite wind turbine blades using ultrasonics. By employing air coupled ultrasonics to facilitate faster and easier scans, we formulated a three step process. Detection was performed with single sided air coupled ultrasonics, and characterization was performed with the help of high frequency contact probes. Severity of the wave was defined with the help of aspect ratio, and several samples with different aspect ratio waves were made. A finite element model for wave propagation in wavy composites was developed, and compared with the experimental results.

## 1. INTRODUCTION

With the introduction of 30 meter blades, and 70 meter blades in prototype for harnessing power above 10Megawatts [1] the design of the blade becomes a crucial factor. Since the blade mass scales as a cube of the turbine radius, lighter, yet stronger materials are employed. Fiberglass composite has phased out some of the conventional materials used in wind turbine manufacturing, but the level of understanding of this material is relatively limited compared to the conventional materials. Defects such as delamination, fiber waviness, lack of infusion, are commonly found in composite wind turbine blades. Since the entire infusion process is manual and hand lay out, it is highly susceptible to human errors and hence these defects become inherent of the manufacturing process.

Waviness in composites has been under investigation since the use of fiberglass and still considerable amount of research efforts are being made. Waviness can be classified into two types, i.e. in-plane waviness and out-of-plane waviness. The wrinkles or marcls can be intrinsic i.e. they can lie within the laminate and have no surface effects or can be extrinsic, i.e. protrude out of the surface and result in surface waviness. Compared to surface waviness, intrinsic waviness is the difficulty to detect due to the flat top and bottom surfaces. The outside of the laminate looks normal and flat, although a critical marcel inside the laminate can degrade it considerably. From an engineering point of view, waviness can be further classified into two types, i.e. uniform waviness and discrete waviness or marcls. Discrete marcls are a tougher challenge and pose a bigger threat to the structure. This paper will concentrate solely on out of plane, and discrete marcls.

Current methods used include visual inspection, high intensity light inspection, contact ultrasonics, and thermography [2]. As with any other engineering problem, it is very difficult to find a method which detects and is highly reliable for all types of defects. Nondestructive evaluation has been used quite extensively for composites and can be extended for wind turbine application. A typical wind turbine blade has three major composite components which are also the backbone of the blade, namely the spar cap, trailing edge and the leading edge. A failure at any of these locations will result in a catastrophic failure of the blade. Thus a critical inspection procedure of these components is vital and necessary.

One of the challenging tasks of implementation and standardization of a technique is the on-site inspection capability. Most of the previously mentioned methods can be performed and tested in a laboratory environment, but on-site inspection is not possible. Although waviness is due to manufacturing variability, it is almost impossible to eliminate them. Moreover, the blades which have already been deployed but were not tested; need to be examined to ensure their design life. This makes the field implementable attribute of the system very important. We propose a scanning technique using air coupled ultrasonic transducers, which is field implementable, fast, and easy to use. The Air medium makes this a completely non-contact method and helps in eliminating the mess created by coupling gel or water. Inspection was initiated in a generic 1.25 inch thick unidirectional composite plate, and was extended to an actual trailing edge sample containing out of plane, discrete marcols. Waviness is defined with the help of aspect ratio, and samples of different aspect ratios were prepared. Inspection was made possible by generating Rayleigh waves on the composite plate using air coupled



transducers of 200 KHz frequency. A method to quantify marcel with the help of aspect ratios was framed and used to determine the severity of the wrinkle or marcel.

## 2. PROBLEM STATEMENT

The main objective of this research is to detect out of plane & discrete marcel in thick composite sections of wind turbine blade and identify a method to quantify marcel with the help of aspect ratios. To accomplish this objective, a two-step method can be used:

**Step 1:** Detect marcel by performing rapid scans and save their spatial location.

**Step 2:** Characterize or quantify the dimensions of the marcel with the help of B scans.

A marcel can be defined in terms of its dimensions with the help of aspect ratio, which is:

$$Ar = \frac{L}{a} \quad (1)$$

Where “a” is the height of the marcel and “L” is the span as shown in Figure (1).

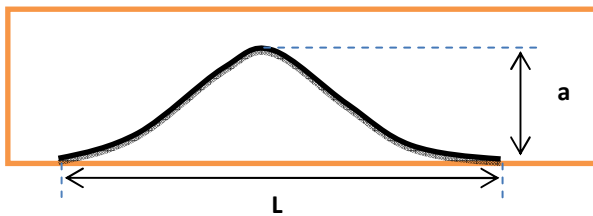


**Fig. 1: Definition of aspect ratio of a discrete marcel**

From the definition of aspect ratio, a marcel with high AR value would be flat compared to a marcel with lower AR value which would be tall and sharp. Lower AR marcel are typically very detrimental compared to high aspect ratios. The range of aspect ratios to be evaluated depends on the thickness of the composite plate under investigation, since an AR 6 marcel

would not have high impact in a 6 inch composite section, compared to an AR 6 marcel in 1.5 inch composite section.

The use of aspect ratio to quantify marcel is not new, and has already been used by J.F.Mandell, et al [6] in the form of wave severity. The non-dimensional form of aspect ratio creates the possibility of two different marcel having the same aspect ratio. But this research limits this paradox by keeping the span of marcel a constant, and therefore making the aspect ratio a unique damage metric.

### 3. BACKGROUND

Although waviness or marcel can be seen as geometrical distortions, a significant change of material properties occurs in the localized region. The localized region of the marcel has lower mechanical properties compared to the entire laminate. The composite laminate is generally defined as orthotropic with 9 independent constants, and the stress-strain relation [10] is given by:

$$\begin{bmatrix} \sigma_1 \\ \sigma_2 \\ \sigma_3 \\ \tau_{23} \\ \tau_{13} \\ \tau_{12} \end{bmatrix} = [C] \begin{bmatrix} \epsilon_1 \\ \epsilon_2 \\ \epsilon_3 \\ \gamma_{23} \\ \gamma_{13} \\ \gamma_{12} \end{bmatrix} \quad (2)$$

Where [C], is called the stiffness matrix and for orthotropic material is given by:

$$[C] = \begin{bmatrix} C_{11} & C_{12} & C_{13} & 0 & 0 & 0 \\ C_{12} & C_{22} & C_{23} & 0 & 0 & 0 \\ C_{13} & C_{23} & C_{33} & 0 & 0 & 0 \\ 0 & 0 & 0 & C_{44} & 0 & 0 \\ 0 & 0 & 0 & 0 & C_{55} & 0 \\ 0 & 0 & 0 & 0 & 0 & C_{66} \end{bmatrix} \quad (3)$$

For plane stress condition the stress strain relations can be reduced to:

$$\begin{bmatrix} \sigma_1 \\ \sigma_2 \\ \tau_{12} \end{bmatrix} = \begin{pmatrix} C_{11} & C_{12} & 0 \\ C_{12} & C_{22} & 0 \\ 0 & 0 & C_{66} \end{pmatrix} \begin{bmatrix} \epsilon_1 \\ \epsilon_2 \\ \gamma_{12} \end{bmatrix} \quad (4)$$

Where,

$$C_{11} = \frac{E_1^2}{E_1 - \nu_{12}^2 E_2} \quad (5)$$

$$C_{22} = \frac{E_1 E_2}{E_1 - \nu_{12}^2 E_2} \quad (6)$$

$$C_{12} = \frac{E_1 E_1 \nu_{12}}{E_1 - \nu_{12}^2 E_2} \quad (7)$$

$$C_{66} = G_{12} \quad (8)$$

Where  $E_1$  and  $E_2$  are the longitudinal and transverse moduli and  $G_{12}$  is the in-plane shear modulus and  $\nu_{12}$  is the major Poisson's ratio.

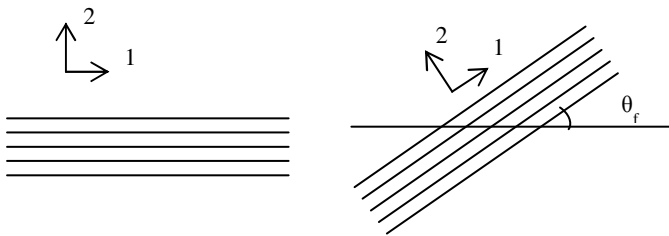


**Fig.2: Axis rotation of angled laminate**

Fiber shearing in the out-of-plane direction can be defined with the help of fiber orientation angle. If the fibers are oriented at an angle with the horizontal, the principal material

coordinate axes can be obtained from the transformation and the resulting six constants are given by the relation:

$$C'_{11} = C_{11}l^4 + 2(C_{12} + 2C_{66})l^2m^2 + C_{22}m^4 \quad (9)$$

$$C'_{22} = C_{11}m^4 + 2(C_{12} + 2C_{66})l^2m^2 + C_{22}l^4 \quad (10)$$

$$C'_{12} = (C_{11} + C_{22} - 4C_{66})l^2m^2 + C_{12}(l^4 + m^4) \quad (11)$$

$$C'_{66} = (C_{11} + C_{22} - 2C_{12} - 2C_{66})l^2m^2 + C_{66}(l^4 + m^4) \quad (12)$$

$$C'_{16} = (C_{11} - C_{12} - 2C_{66})l^3m + (C_{11} - C_{12} - 2C_{66})m^3l \quad (13)$$

$$C'_{26} = (C_{11} - C_{12} - 2C_{66})m^3l + (C_{11} - C_{12} - 2C_{66})l^3m \quad (14)$$

Where  $l$  and  $m$  are the direction cosines,

$m = \sin(\theta_f)$  and  $l = \cos(\theta_f)$ , and  $\theta_f$  is the angle between the fiber angle and horizontal as shown in Figure (2).

For smaller displacements, for the case of a plane wave the Christoffel equation can be obtained from the equation of motion [14][15] as

$$\Omega(m) = \det |C_{ijkl}m_jm_l - \rho\delta_{ik}| \quad (15)$$

Where  $C_{ijkl}$  is the stiffness tensor and  $\delta_{ik}$  is the Kronecker delta function.

By substituting the transformed equations in Christoffel Equation we obtain:

$$\Omega(m) = \begin{vmatrix} m^2\Gamma_{11} - \rho & m^2\Gamma_{12} \\ m^2\Gamma_{12} & m^2\Gamma_{22} - \rho \end{vmatrix} \quad (16)$$

In terms of phase velocity it can be written as:

$$\Omega(c) = \begin{vmatrix} \Gamma_{11} - \rho c^2 & \Gamma_{12} \\ \Gamma_{12} & \Gamma_{22} - \rho c^2 \end{vmatrix} = 0 \quad (17)$$

Where

$$\Gamma_{11} = C_{11}\alpha^2 + 2C_{16}\alpha\beta + C_{66}\beta^2 \quad (18)$$

$$\Gamma_{12} = C_{16}\alpha^2 + (C_{12} + C_{66})\alpha\beta + C_{26}\beta^2 \quad (19)$$

$$\Gamma_{22} = C_{66}\alpha^2 + 2C_{26}\alpha\beta + C_{22}\beta^2 \quad (20)$$

$$\alpha = \cos \theta_p; \beta = \sin \theta_p$$

Where,  $\theta_p$  is the propagation angle with respect to the horizontal.

This can be solved for the velocity as:

$$\rho c^2 = \frac{a_1 \pm \sqrt{a_1^2 - 4a_2}}{2} \quad (21)$$

The positive root denoting the compressional wave solution and the negative root denoting the shear wave velocity. For horizontal propagation, or  $\theta_p = 0^0$ , we can change the fiber

orientation from 0 to 90 and determine the shear and longitudinal wave velocities. The variation of velocity with changes in fiber angle is shown in Figure (3).

The laminate under investigation has thick plies compared to a generic glass fiber composite plate. Each ply is 0.7mm, and hence the effect of wave propagation in anisotropic media is prominently influenced by the individual layers. To include the effect of thick layers in wave propagation, one has to change the fundamental field equations. This was derived by Stoneley, 1949 [11] for transversely isotropic media and is given by,

$$R = \Gamma_1 \Pi_2 + \Gamma_2 \Pi_1 = 0 \quad (22)$$

Where,

$$\Gamma_1 = [-\gamma_1 v_1 C_{11} + C_{12}k]; \Pi_1 = [v_1 + \gamma_1 k] \quad (23)$$

$$\Gamma_2 = [-\gamma_2 v_2 C_{11} + C_{12}k]; \Pi_2 = [v_2 + \gamma_2 k] \quad (24)$$

Where,

$$v_1^2 = \frac{-M_1}{2C_{11}C_{55}} + \frac{M_3}{2C_{11}C_{55}} \quad (25)$$

$$v_2^2 = \frac{-M_1}{2C_{11}C_{55}} - \frac{M_3}{2C_{11}C_{55}} \quad (26)$$

$v_1^2$  Corresponds to the compressional wave speed, and  $v_2^2$  corresponds to the shear wave speed.

The various M factors are given by:

$$M_3^2 = M_1^2 - 4M_2C_{11}C_{55} \quad (27)$$

$$M_1 = C_{11}(\rho_1\omega^2 - C_{22}k^2) + C_{55}(\rho_1\omega^2 - C_{55}k^2) + k^2G^2 \quad (28)$$

$$M_2 = (\rho_1\omega^2 - C_{22}k^2)(\rho_1\omega^2 - C_{55}k^2) \quad (29)$$

And the amplitude ratio's,  $\gamma_1$  and  $\gamma_2$  are given by:

$$\gamma_1 = \frac{C_{55}v_1^2 - C_{22}k^2 + \rho_1\omega^2}{k v_1 G} \quad (30)$$

$$\gamma_2 = \frac{C_{55}v_2^2 - C_{22}k^2 + \rho_2\omega^2}{k v_2 G} \quad (31)$$

And the wave number k is given by;

$$k = \omega/C_R$$

Where  $C_R$  is given by the Rayleigh wave velocity. By solving Equation (22), The Rayleigh wave speed for a particular frequency can be obtained. This solution can be extended to obtain the dispersion effect of Rayleigh wave.

The extant literature on waviness suggests the degradation of material properties as the fiber orientation increases. Daniel Adams, 1994 [7] showed that for a composite laminate, the strength reduction is dependent on the number of layers of the marcel. In his investigation he

reported that a 35% strength reduction was observed when the marcel contains greater than 33% of the straight layers, for a particular aspect ratio.

In application to wind turbine blades, which typically has thicker composite sections (from .25 inches to 5 inches), the presence of a marcel has a much prominent effect on the fatigue life of the blade. Murri [5] was able to show that Fatigue life of a laminate with waviness decreased by a factor of  $10^2$  to  $10^3$ . Such a decrease in the fatigue life of the blade would raise questions over economic investments and the manufacturing abilities. A tight quality control method is necessary to prevent catastrophic failure of blades in service.

#### **4. SAMPLES USED**

Initial investigation of this research was performed on a generic 1.25 inch thick unidirectional glass-fiber laminate with engineered defects, and control samples. Since this investigation limits to discrete-out of plane waviness or marcel, wedges of desired aspect ratio were cast out of epoxy molds and were inserted in between the fabric during the resin infusion process. Intrinsic marcel were created by supporting the top and bottom with flat plates under pressure. This is an important step since out of plane marcel protruding out of the laminate can be visually detected. On the other hand intrinsic marcel which lie inside a laminate and is flat on the top and bottom are much difficult to detect.

This research focuses on detecting and characterizing intrinsic, discrete, and out-of-plane marcel. To confirm the findings, real trailing edge samples with engineered marcel were created. These samples emulate a field test, and help in optimizing parameters such as



frequency, distance of separation between transducers etc. The list of samples used for testing and their specifications are described in Table I.

**TABLE II: List of Samples used for experiments and their details**

Sample Name	Aspect ratios	Depth information
<b>Generic wavy laminates</b>		
<b>WS-01</b>	6, 10, 14	6mm
<b>WS-02</b>	8, 12, 16	6mm
<b>WS-03</b>	6, 10, 14	12mm
<b>WS-04</b>	8, 12, 16	12mm
<b>WS-05</b>	6, 10, 14	18mm
<b>WS-06</b>	8, 12, 16	18mm
<b>Trailing edge samples</b>		
<b>TE-H</b>	18	Inner UD layer
<b>TE-I</b>	9	Outer UD layer
<b>TE-J</b>	13	Outer UD layer
<b>TE-K</b>	17	Outer UD layer
<b>TE-L</b>	18	Outer UD layer
<b>TE-M</b>	9	Inner UD layer
<b>TE-N</b>	13	Inner UD layer

Six set of generic wavy laminates were manufactured with six different aspect ratios and 3 different depth information. All the laminates are 1.125 inch thick, and the depth information corresponds to the position of the marcel with respect to the top surface. Laminates WS-01, WS-03, and WS-05 have the same aspect ratio marcel, but at different depth from the top surface. Similarly the even numbered samples contain three marcel each at different depth information.

The trailing edge has a different construction compared to the generic composite laminate. It has a symmetric construction with bi-axial layers and unidirectional layers of glass fiber. The two halves are bonded together by adhesive. The “UD” layer corresponds to the

unidirectional fiberglass layers, and the “Biax” refers to the bi-axial 45 degree cross weave layers. Typically the trailing edge (TE) samples were 1.5 inches thick, and 7 TE samples with three different aspect ratios were fabricated. The inner UD layers are closer to the adhesive bond, i.e. farther from the top surface, and out UD layers are closer to the top surface.

High magnification micrographs (8 x magnifications) of two different marcells are shown in Figure (6) and Figure (7). The distortion of each ply can be seen clearly in these photographs.

## **5. EXPERIMENTAL SETUP**

This investigation was conducted in two parts and two different setups were utilized for all the experiments. The first part consists of “proof of concept” approach in a laboratory based system, and the second consists of developing a stand-alone, field implementable system. Both the setups are explained in detail below.

### **5.1. LABORATORY BASED SYSTEM**

The lab based system was used as a proof-of-concept tool, to test the abilities of a Rayleigh wave based setup in a lab environment. The schematic of the setup is shown in Figure (4).

The setup consists of a three axis X-Y-Z scanner to perform high resolution C Scan (Signal amplitude vs. spatial location) and B scan (depth time of flight vs. spatial location), and a pulser receiver is used to drive a pair of 200KHz air coupled ULTRAN transducers at 100 KHz PRF. The movement of the scanner is controlled by a motion controller and the output signal waveform from the pulse receiver is sent to a computer for data analysis. The software in computer enables the motion controller to be easily interfaced to produce the necessary B and C scans.

## **5.2. STANDALONE SYSTEM**

The standalone system is shown in Figure (5), consists of the Olympus EPOCH XT with B scan capability, connected to a three wheeled scanner developed for this purpose.. A pair of 200 KHz, non-focused, air coupled ULTRAN transducers was mounted on the scanner, and used for all the characterization portion of this investigation. This instrument enables high resolution B scans over a small area and the ability to quantify marcells. A three wheeled scanner was designed from scratch keeping in mind the contours over which the scanner has to travel, ease of use and cost effectiveness.

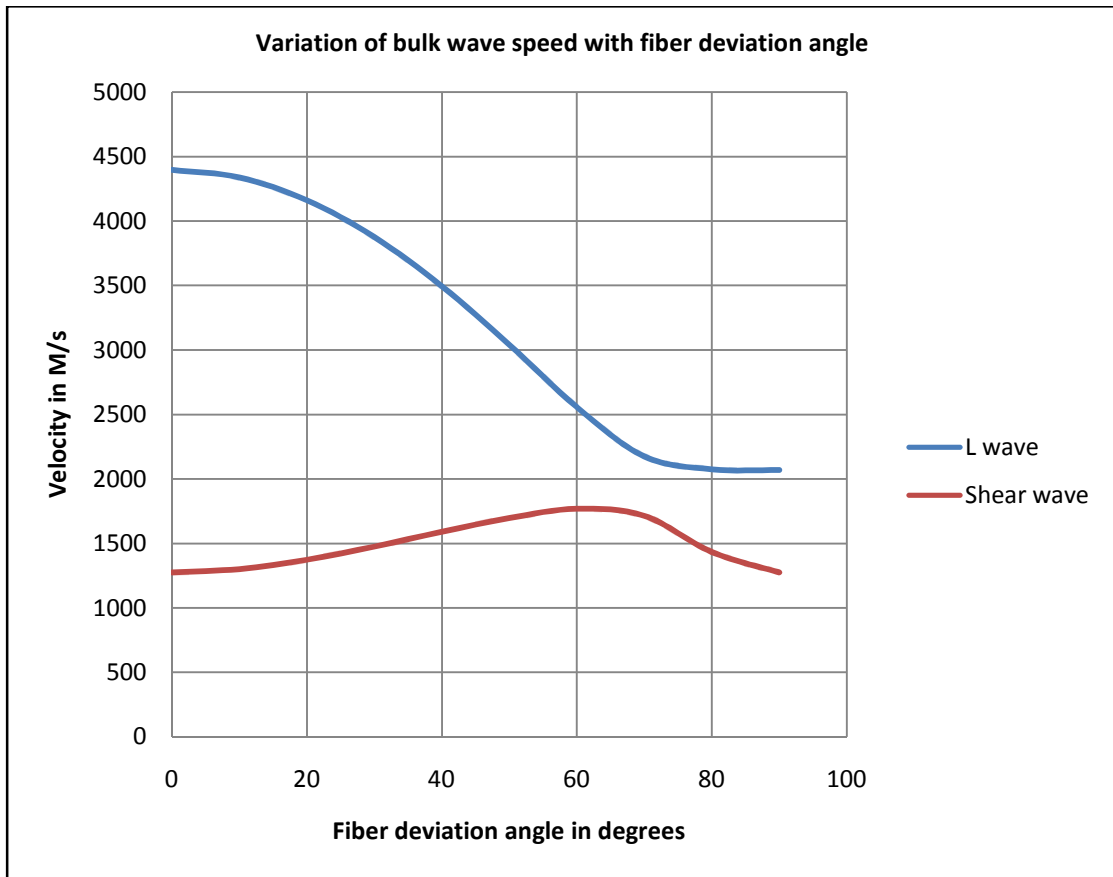


**Fig.3: Variation of bulk wave speed (longitudinal and shear) with fiber deviation angle**

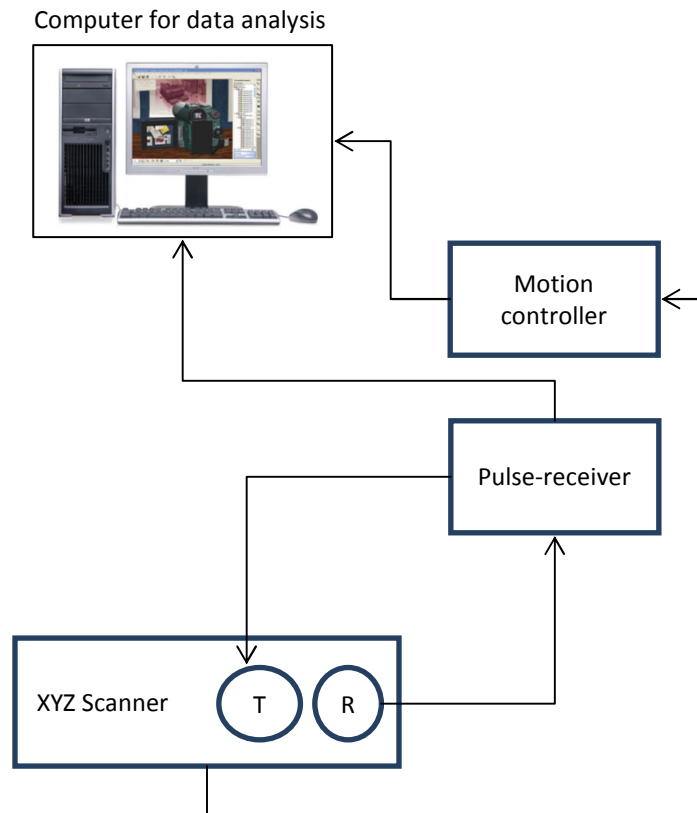


**Fig.4: Schematic of the Laboratory based scanning system used as a proof-of-concept tool.**



**Fig.5: Schematic of the standalone scanning system.**

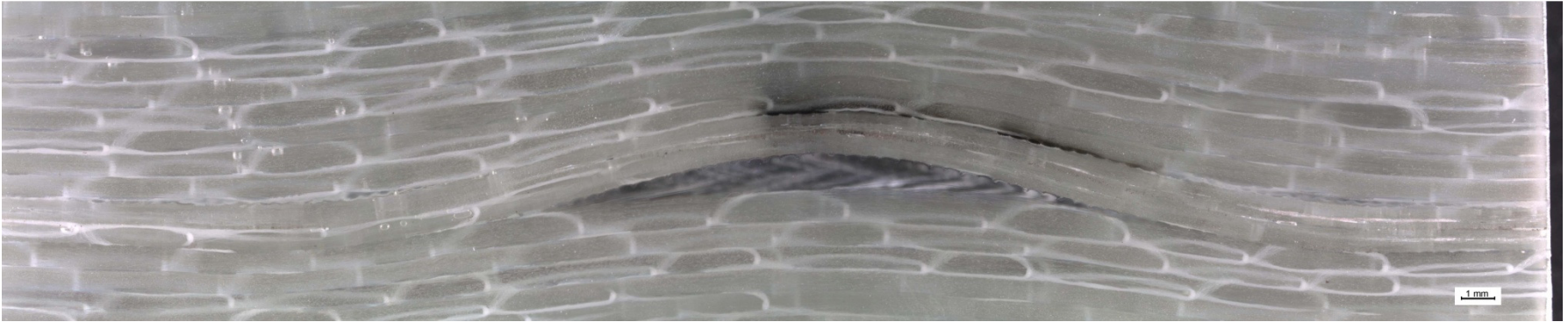


**Fig.6: 8x micrograph of discrete out of plane marcel of AR 14**

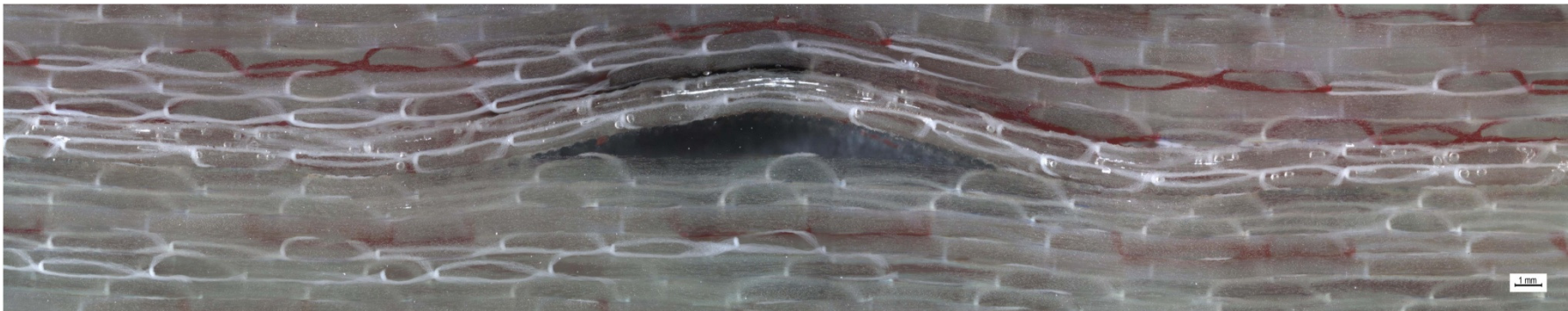


**Fig.7: 8x micrograph of discrete out of plane marcel of AR 10**

## 6. RESULTS

### 6.1. DETECTION - Part A

A single sided pitch catch approach was used for detection of marcel. By inclining the transducers at an angle beyond the 2<sup>nd</sup> critical angle, Rayleigh wave was generated on the surface of the samples. A constant distance between the transducers was maintained at 4 inches. B scans were performed by translating the scanner or transducer setup across the wave. The direction of Rayleigh wave propagation was parallel to the direction of the marcel, and perpendicular to the direction of the unidirectional fibers. This is explained schematically in Figure (8).

From experimental observations two types of discrete, intrinsic, out of plane marcel can be identified. The upward pointing marcel and the downward pointing marcel. Figure (7.b) shows the C-scan image of marcel of AR 8 placed at 6mm depth. The effect of the marcel on wave propagation can be noticed as a reduction of Rayleigh wave amplitude in the localized region. The other striations in the scan are a result of edge interference of the sample. Figure (7.a) shows the C scan image of a downward pointing marcel of the AR 8 placed at 12mm depth.

Compared to the upward pointing marcel, an increase in Rayleigh wave amplitude was noticed for the downward pointing marcel. To further examine the amplitude phenomenon, a high resolution B scan was performed on both types of marcel. A change in velocity, amplitude and phase shift was observed while translating over the marcel. The observations recorded for these two marcel are tabulated in Table II.

Based on the preliminary investigation a three step method was proposed to achieve the previously defined objectives of the research:

**Step 1:** Perform large area scans using air coupled ultrasonics to detect marcel

**Step 2:** Once marcel is detected they are characterized based on their orientation, i.e. upward or downward pointing marcel.

**Step 3:** B-scan is performed to determine the velocity, amplitude and phase shift. These values are recorded and compared to the standardized sample set. An approximate aspect ratio number is determined based on range where the number fits in.

Using this three step method, any marcel, of any orientation and aspect ratio can be detected, characterized based on standardized parameters such as frequency, distance of separation between transducers and angle of orientation of the transducers. Considering the above factors, the 2<sup>nd</sup> step of detection was initiated.

## **6.2. DETECTION – Part B**

To refine the method, a standard set of samples were manufactured. The samples as listed in Table I were created to form a standard set of values to which one can compare a marcel of unknown aspect ratio and determine an approximate value for the aspect ratio. Typically, the thickness of composite sections of the wind turbine ranges from 0.25 inches to 5 inches. The range of aspect ratio considered detrimental would range from 6 to 16. Along with the AR value, the effect of depth on experiments was also studied by placing marcel at

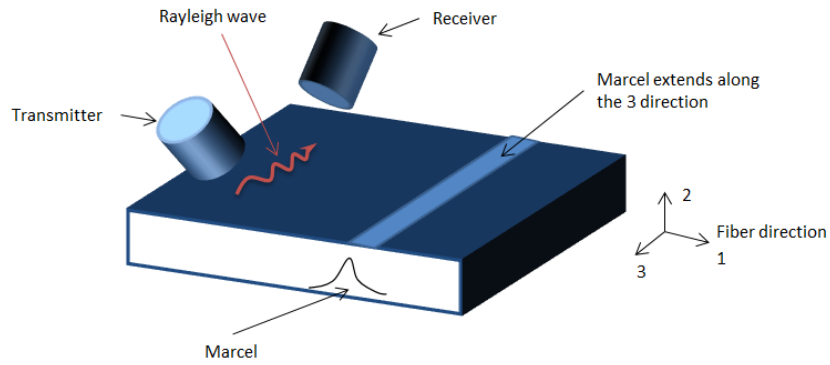


different depth in the standard samples. The aspect ratios and the depth information are listed in TABLE I.

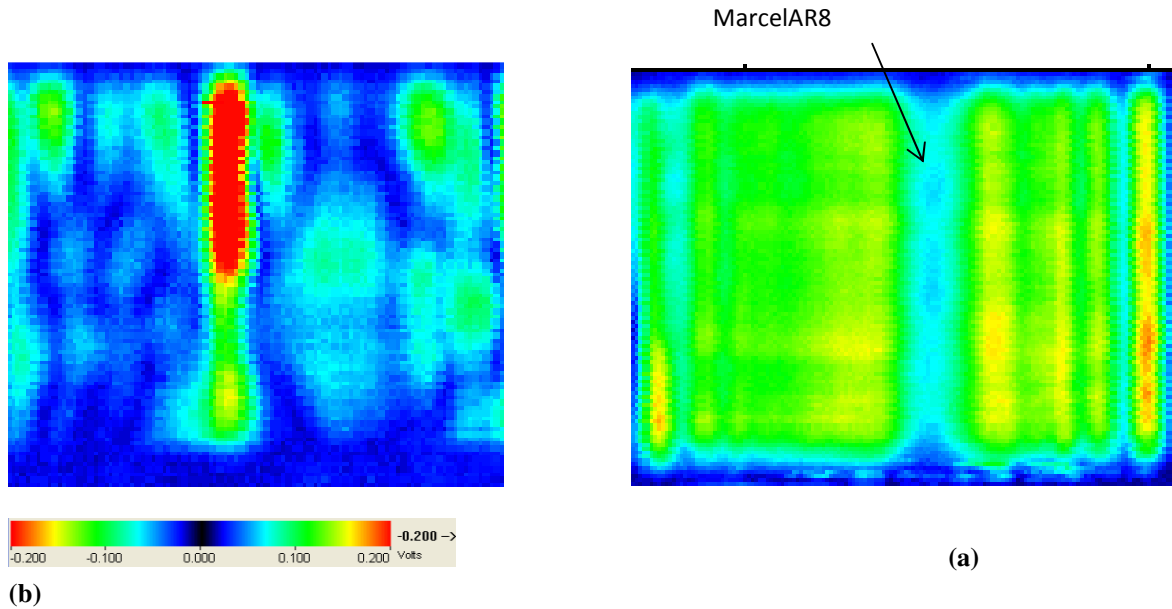
Once the standard samples were manufactured, they were tested with the laboratory setup shown in Section 5. C scan results of the six samples containing three marcel each is shown in Figure (10. a) through Figure (10.f).

The marcel in each case is identified by the white circle marked on the image. Striations due to dry fibers and non-uniformity in material can also be observed in samples WS-02, WS-3, WS-05, which do not typically occur in factory manufactured samples. The possibility of a false detection can be eliminated since; the method does not work exclusively on amplitude, but works on other factors such as velocity, frequency etc. From the C Scan results, it is evident that the maximum sensitivity for detection is in the AR range of 6-14, for any marcel at a depth of 12mm. Beyond 12mm depth the detection sensitivity decreases and reliability of the system decreases. As seen in Figure (10.f) for sample WS-06, AR 12, and AR16 are difficult to detect at 18mm depth.

To further test the effectiveness of detection method, the trailing edge samples were tested using the lab setup. Figure (11.a) through Figure (11.d) shows the C scan results of the TE samples listed in TABLE I. All the marcel were detected using this method, including the ones placed on the inner UD layer of TE. Hence the sensitivity to depth was also confirmed in TE samples. As seen in the detection results, the reliability, repeatability and effectiveness of the method is very high compared to other detection techniques.





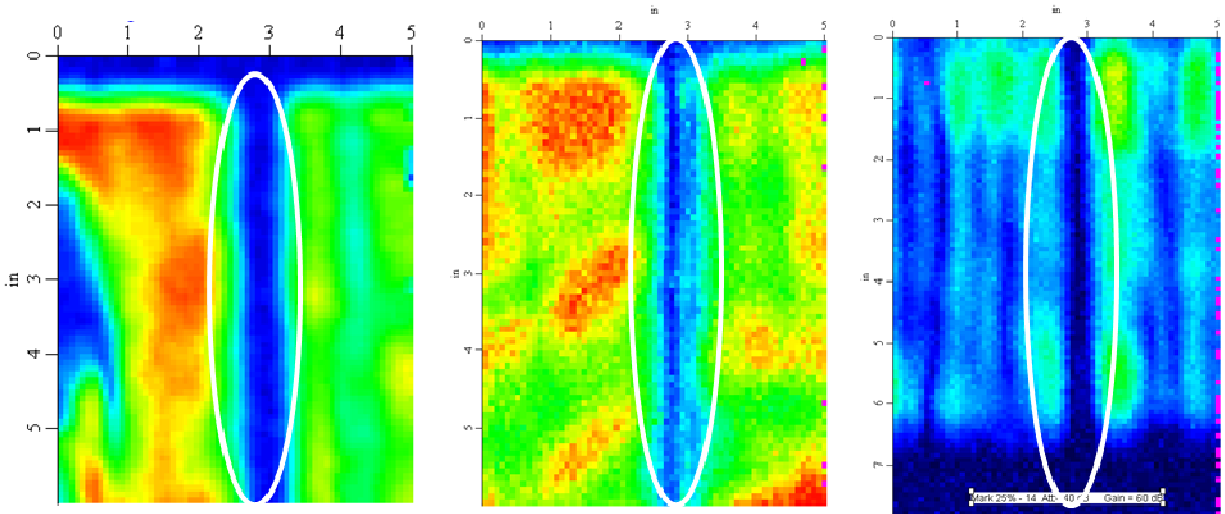
**Fig. 8: Schematic of experimental setup. Wave propagation direction is parallel to the direction of marcel and perpendicular to the direction of unidirectional fibers.**



**Fig. 9: C-Scan marcel of AR 8, (a) Downward pointing marcel, (b) Upward pointing marcel**

**TABLE.II: Summary of upward and downward pointing marcel characteristics.**

Wave type	Name	Signal Amplitude	Wave Velocity
	Upward pointing wave	Decrease in amplitude	Increase in velocity, phase shift observed
	Downward pointing wave	Increase in amplitude	Decrease in velocity, phase shift observed

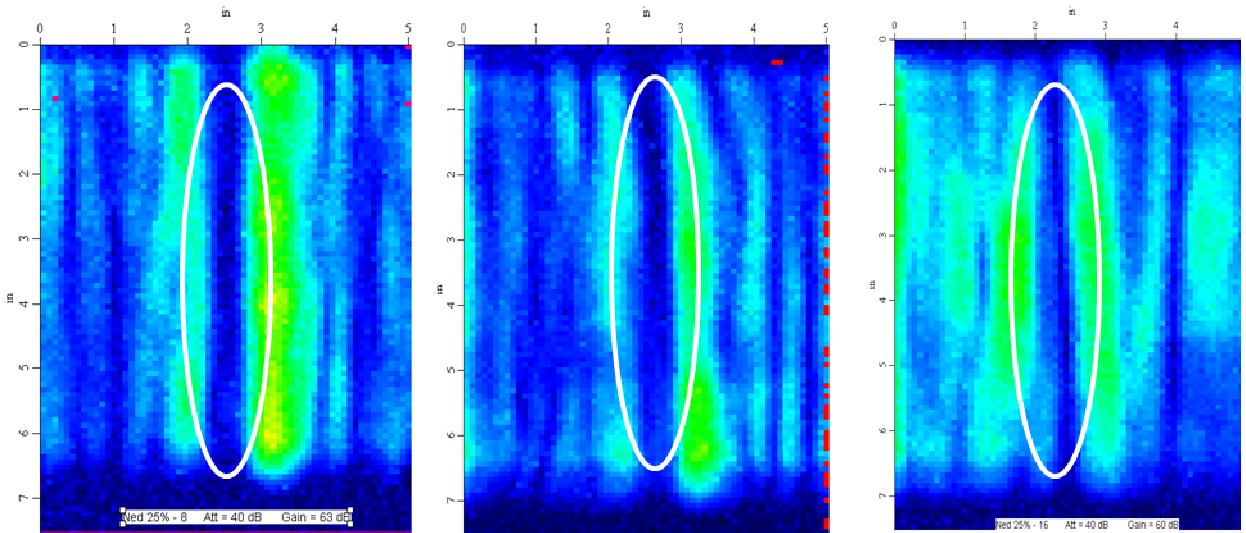


WS-01: AR 6

WS-01: AR 10

WS-01: AR 14

Fig.10 (a)

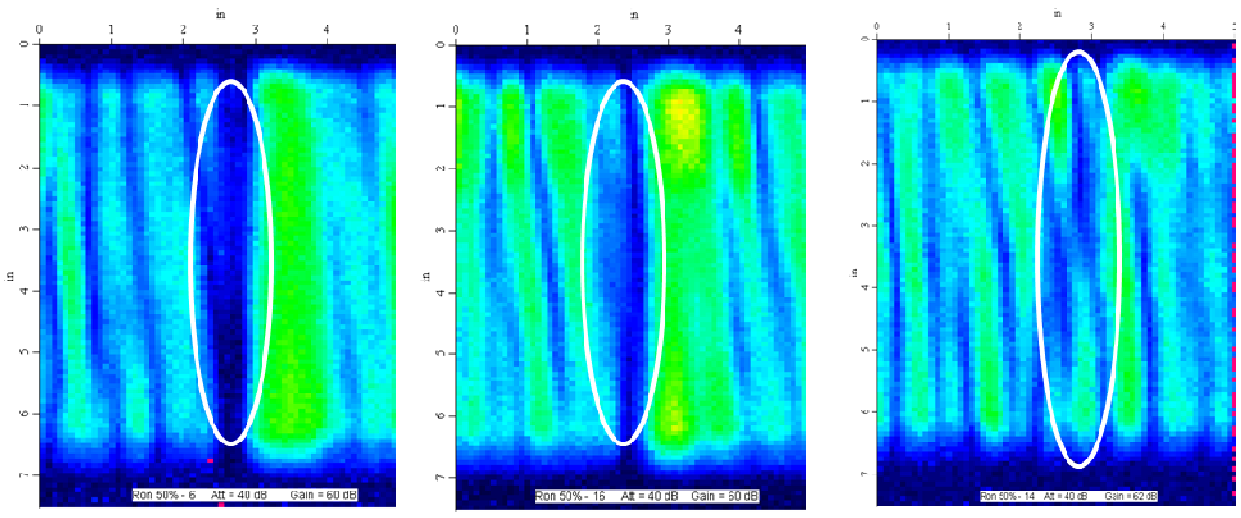


WS-02 AR 8

WS-02 AR 12

WS-02 AR 16

Fig.10 (b)

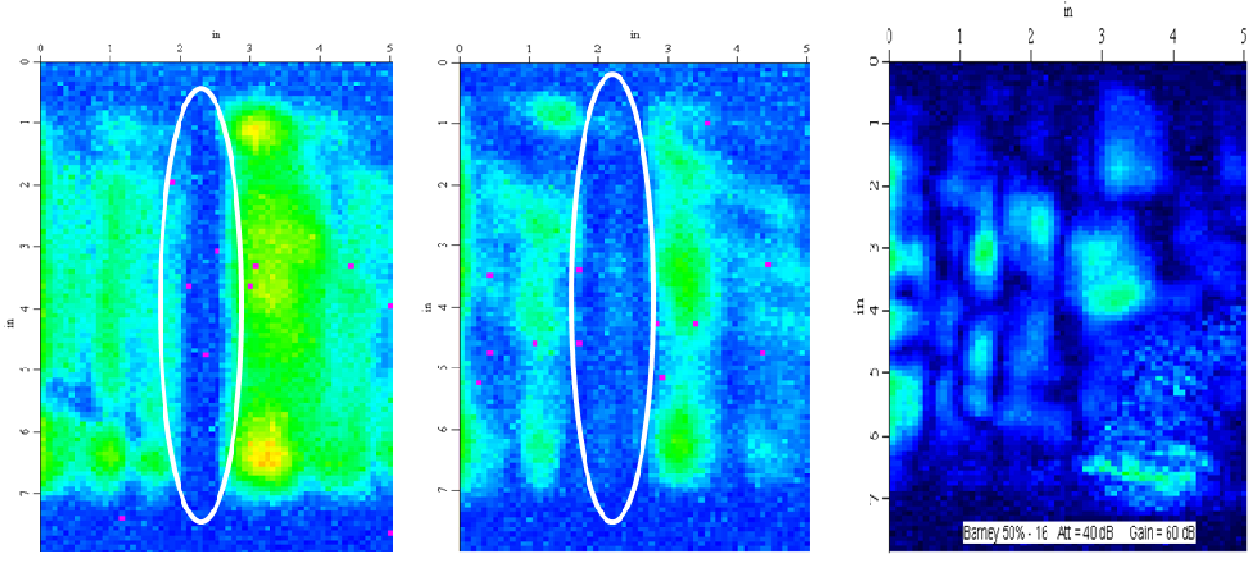


WS-03 AR 6

WS-03 AR 10

WS-03 AR 14

Fig.10 (c)



WS-04 AR 8

WS-04 AR 12

WS-04 AR 16

Fig.10 (d)

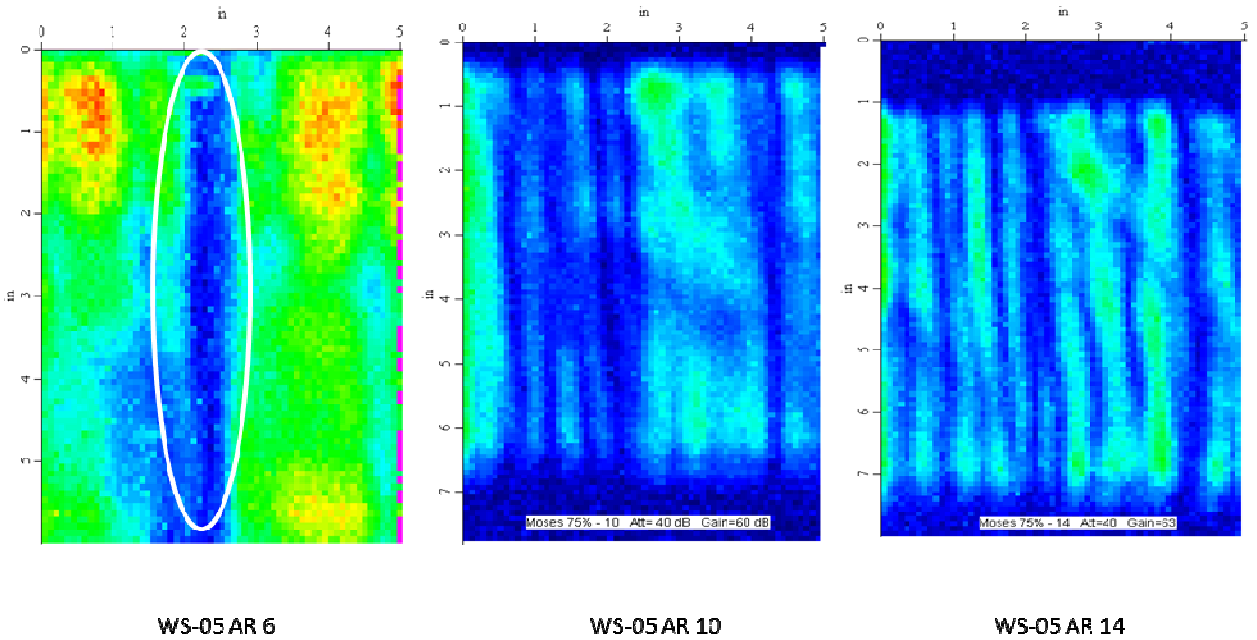


Fig.10 (e)

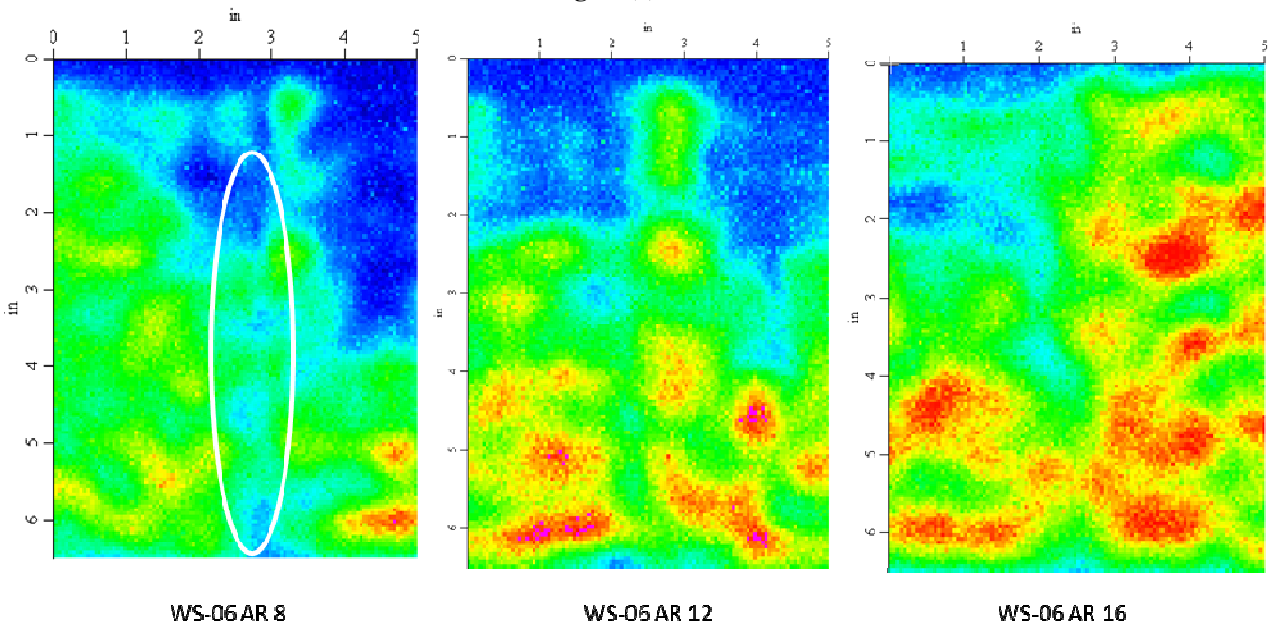


Fig.10 (f)

Fig.10: C-Scan results of standard samples using laboratory based system for (a) WS-01, (b) WS-02, (c) WS-03, (d) WS-04, (e) WS-05, and (f) WS-06. The detected marcel's are marked with a white circle.

### 6.3. CHARACTERIZATION

The second objective of this research is to quantify the detected marcel with the help of aspect ratio. Once the orientation of the marcel is determined, a high resolution B scan in the vicinity of the marcel would yield various parameters such as change in Time of flight (TOF) and amplitude which are required to quantify the marcel. As mentioned earlier, high resolution B scans using the stand alone setup as described in Section 5 were performed on the standard set of samples, and the results are shown in Table III through Table VII.

The TOF change over the marcel is obtained from the B Scan and is stored for all the standard set of samples. This change in TOF is termed as damage index number, and is useful to determine a marcel of unknown aspect ratio. The relative change in TOF was measured by recording the TOF value in good region (GR) and in the defective region (DR) or over the marcel. These are denoted as GR and DR in Table III through VII.

### 6.4. CHARACTERIZATION DISCUSSIONS

From Table III – Table VII, we can notice that maximum sensitivity is at 6mm from the top surface, and this is consistent with the fact that Rayleigh wave displacements are maximum at the surface and decreases with depth. It is also observed that AR 16 is very flat compared to AR14, and hence determining the difference in TOF is difficult.

As we see from Table III and Table IV for sample WS-01 and WS-02, the damage index numbers for 8, 12, and 16 fit in-between the numbers for 6, 10, and 14. Therefore, one can perform the B-scan on an unknown marcel, and with the help of the damage index (DI)

number for that marcel, comparing it to the standard DI number; we can determine the aspect ratio of the unknown marcel. Table V, WS-03 shows B scan DI for 12mm depth. We can notice the inconsistency for AR 14, since the sensitivity with depth decreases. From Table VI, for WS-04, no consistent result was obtained for AR 16 and was reported as 0. Similarly AR 12 did not give consistent results. The decrease in sensitivity is evident for sample WS-05 in Table VI, i.e. 18mm depth. At 12mm and 18mm, the TOF change decreases but creates a paradox, since two different aspect ratios can have the same TOF change at different depths. Although the possibility of detecting marcel of any aspect ratio at depth, i.e. 6 to 12mm is high and evident from the results in Section 6.2, the ability to characterize a marcel is constrained to 6mm, which is a little less than the wavelength of the Rayleigh wave. This method works at best for the trailing edge, since the composite layer on each side is only 7-8mm. But for spar cap sections which are very thick compared to trailing edge sections, the Rayleigh wave-air coupled system can be used for large area scans to detect marcel but characterization will not be possible. A plot of Damage index (DI) vs. Aspect ratio can be seen in Figure (12), which shows the detection range for the proposed method. The air coupled transducers have a frequency constraint and work best at lower frequencies, i.e. less than 400KHz. High resolution B scans on trailing edge were repeated at 2.25MHz with contact transducers to test the influence of frequency. The B scan results of the TE samples are shown in Figure (13.a) to Figure (13.c). All the marcel from H through N, as listed in Table I were detected and characterized using the Rayleigh wave based air coupled scanning system. But the high frequency B scan method is limited by depth, since the wavelength of Rayleigh wave is very short compared to 200 KHz. Hence this method is very effective for thin spar cap samples and trailing edges.

**TABLE.III: B Scan of WS-01**

<b>Sample: WS-01</b>			
<b>AR</b>	<b>Region</b>	<b>TOF change in micro sec</b>	<b>Damage index number</b>
<b>6</b>	GR	20.71	15.45
	DR	5.26	
<b>10</b>	GR	20.11	8
	DR	12.15	
<b>14</b>	GR	18.043	2.35
	DR	15.69	

**TABLE.VI: B Scan of WS-04**

<b>Sample: WS-04</b>			
<b>AR</b>	<b>Region</b>	<b>TOF change in micro sec</b>	<b>Damage index number</b>
<b>8</b>	GR	22.12	3.2
	DR	18.92	
<b>12</b>	GR	22.67	4.74
	DR	17.93	
<b>16</b>	GR	0	0
	DR	0	

**TABLE.IV: B Scan of WS-02**

<b>Sample: WS-02</b>			
<b>AR</b>	<b>Region</b>	<b>TOF change in micro sec</b>	<b>Damage index number</b>
<b>8</b>	GR	19.27	9.4
	DR	9.88	
<b>12</b>	GR	18.89	3.36
	DR	15.53	
<b>16</b>	GR	19.33	4.75
	DR	14.58	

**TABLE.VII: B Scan of WS-05**

<b>Sample: WS-05</b>			
<b>AR</b>	<b>Region</b>	<b>TOF change in micro sec</b>	<b>Damage index number</b>
<b>6</b>	GR	21.68	3.2
	DR	18.48	
<b>10</b>	GR	21.64	1.7
	DR	19.95	
<b>14</b>	GR	21.28	1.28
	DR	20.01	

**TABLE.V: B Scan of WS-03**

<b>Sample: WS-03</b>			
<b>AR</b>	<b>Region</b>	<b>TOF change in micro sec</b>	<b>Damage index number</b>
<b>6</b>	GR	21.35	9
	DR	12.46	
<b>10</b>	GR	20.88	1.7
	DR	19.19	
<b>14</b>	GR	20.32	1.1
	DR	19.28	



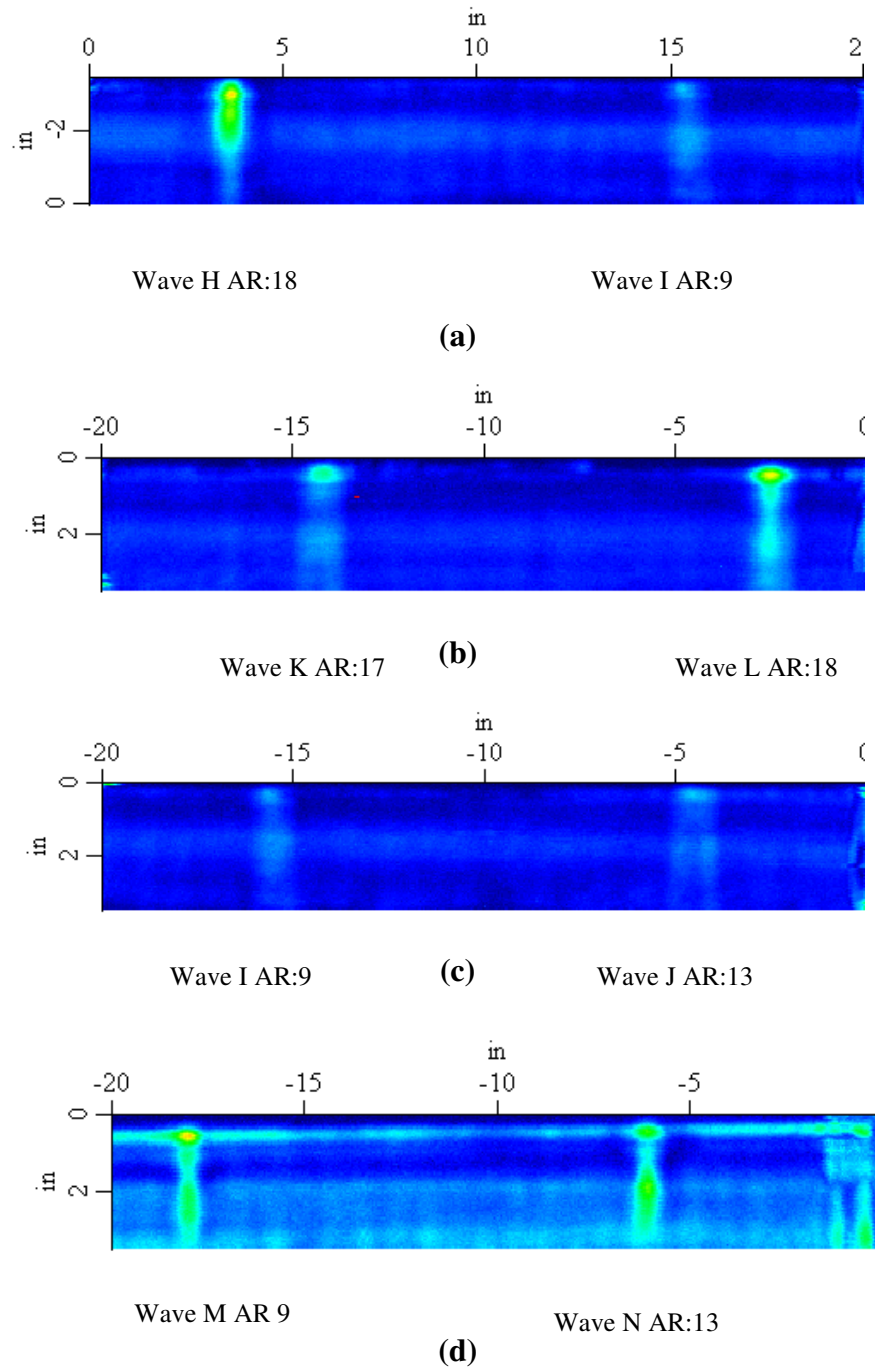
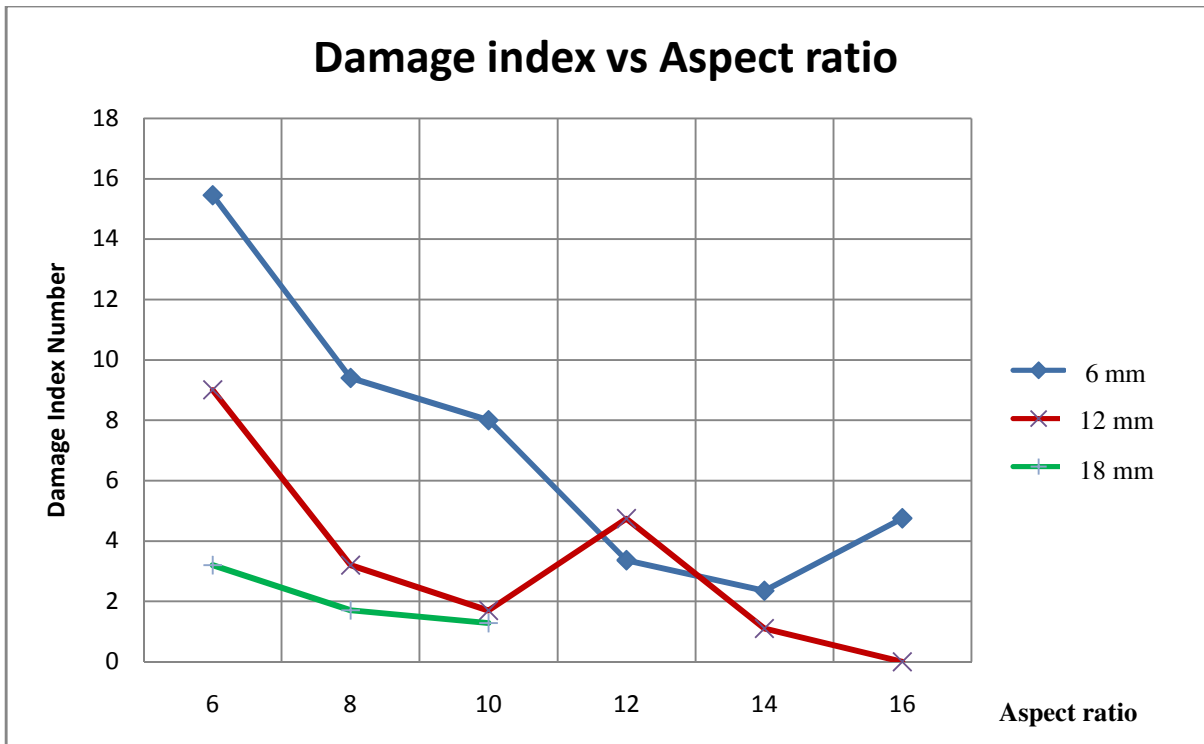
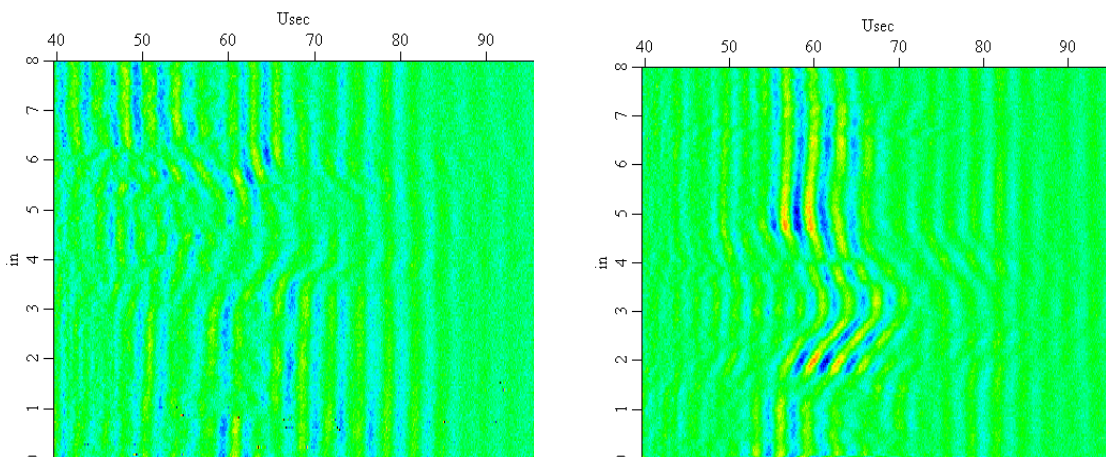


Fig.11: C-Scan results of trailing edge samples, (a) Wave H, I (b) Wave K, L (c) Wave I, J (d) Wave M, N



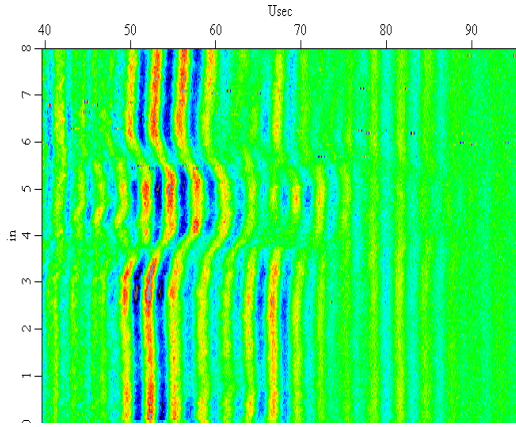
**Fig.12: Damage index vs. Aspect ratio for marcel at 6, 12 and 18mm depth. Information from Table 2-6 was used to plot this.**



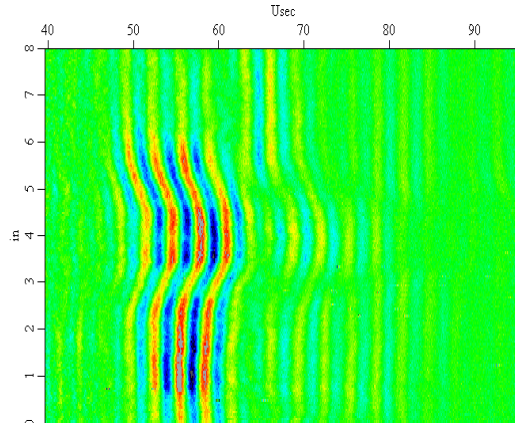
Wave H AR: 18 Inner UD

Wave L: AR 18

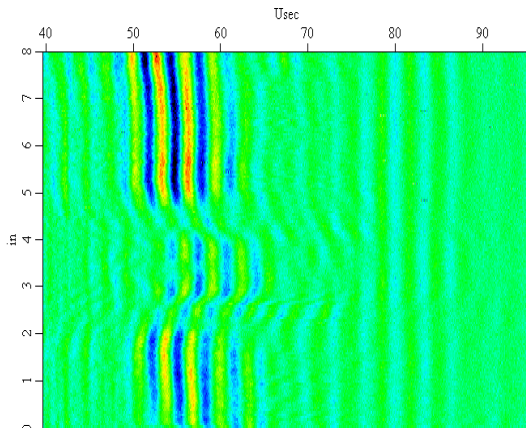
**Fig.13 (a)**



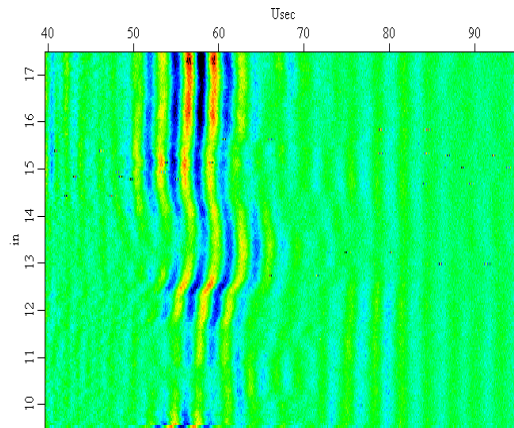
Wave J AR: 13



Wave N AR: 13 Inner UD

**Fig.13 (b)**

Wave I AR: 9



Wave M AR: 9 Inner UD

**Fig.13 (c)**

**Fig.13: High resolution B scans using 2.25 MHz contact transducers. (a) Wave H, L (b) Wave J, N (c) Wave I, M**

## 7. FINITE ELEMENT MODELING

To understand the physics behind the interaction between elastic wave and marcel, finite element method was used. A 2-D model of a generic unidirectional composite plate with intrinsic, discrete, out-of-plane marcel was modeled using ANSYS 13 as shown in Figure (14).

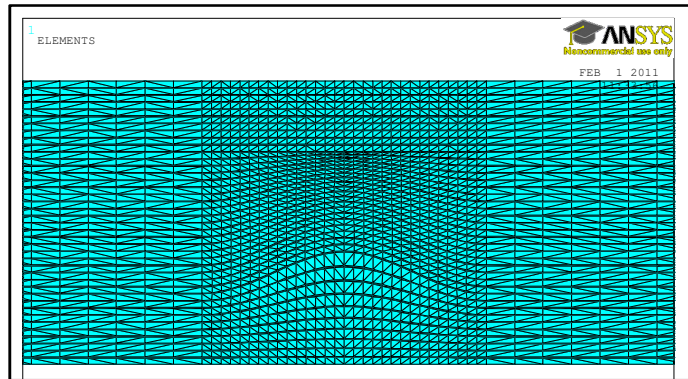


**Fig.14: 2-D ANSYS model of discrete, out-of-plane waviness**

The finite element model consists of individual glass-fiber plies and a layer of epoxy between two plies. The glass-fiber plies were attributed with the global laminate material property, and the layer of epoxy was given the material property of the epoxy used for infusion. A discrete marcel was constructed by geometrically distorting individual plies in Y direction in the XY (or 12) plane. The change in properties was not inputted individually, since mathematically the geometrical distortions create the change in properties in the local region. 2D PLANE 183 (8-node) element with plane strain condition was used to create the model representing a thick structure in the Z-direction. The material properties used for numerical modeling are listed in Table VIII.

**TABLE.VIII: Material properties of laminate and epoxy used for numerical modeling.**

<b>Properties of Laminate</b>	<b>Value in GPa</b>
$E_x$	44.68
$E_y$	6.90
$E_z$	6.90
$\nu_{xy}$	0.280
$\nu_{yz}$	0.355
$\nu_{xz}$	0.280
$G_{xy}$	3.06
$G_{xz}$	3.33
$G_{yz}$	3.109
$\rho$	1990 Kg/m <sup>3</sup>
<b>Properties of Epoxy</b>	
$E_x$	3.0
$\nu_{xy}$	0.38
$\rho$	1200 Kg/m <sup>3</sup>

As an initial step to optimize frequency, wave propagation analysis was performed at 100 KHz, 200 KHz and the waveform was collected for 200 microseconds. B scans were performed by moving the exciting node for each step by running it in a loop. The B scans helped in comparing the numerical results with experimental data. A numerically simulated A-scan of the Rayleigh wave is shown in Figure (15). A TOF measurement in the numerical model showed that the numerical and experimentally observed velocities matched well. The numerical TOF shown in the Figure (15) might be different, due to the different travel path of the ultrasonic wave. In experiment, air coupled transducers were used, where the ultrasonic wave takes a slower travel path through air media. But this was not replicated in the finite element model, where no fluid structure interaction was modeled. An extended analysis of the wave propagation revealed the presence of a secondary mode. When the thickness of individual plies was decreased, the presence of a secondary mode traveling faster than the primary mode was observed. Figure (23) and Figure (24) show the wave propagation analysis for different thickness of individual fibers.

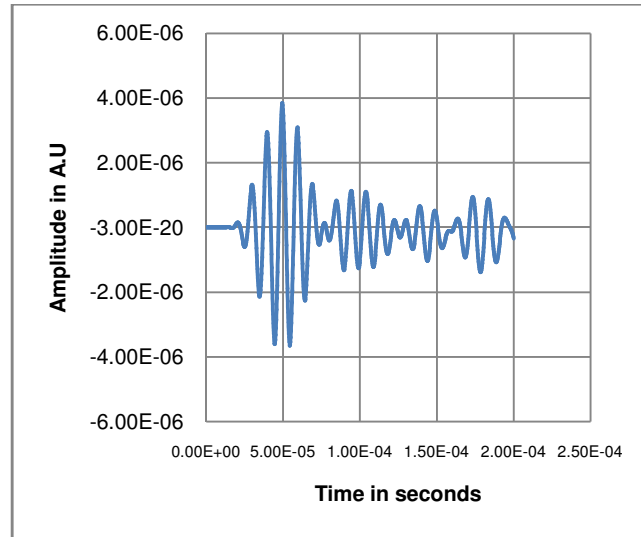


**Fig.15: Numerical A-Scan of Rayleigh wave.**

## 7.1. NUMERICAL B SCAN

The model explained in the previous section was used to perform numerical B scans for an upward pointing marcel of aspect ratios 6. The initial investigation involved studying the influence of frequency and optimizing it. Figure (16) shows a B scan of 100 KHz and Figure (17) shows B scan of 200 KHz for a marcel of AR 6.

As seen in Figure (17), better sensitivity in terms of TOF and amplitude change can be observed for the 200 KHz numerical B scan. All the consecutive numerical simulations involved the usage of 200 KHz. The influence of depth on detection was performed by modeling the marcel at 6, 12 and 18mm. The B Scan of each case is shown in Figure (17), Figure (18) and Figure (19).

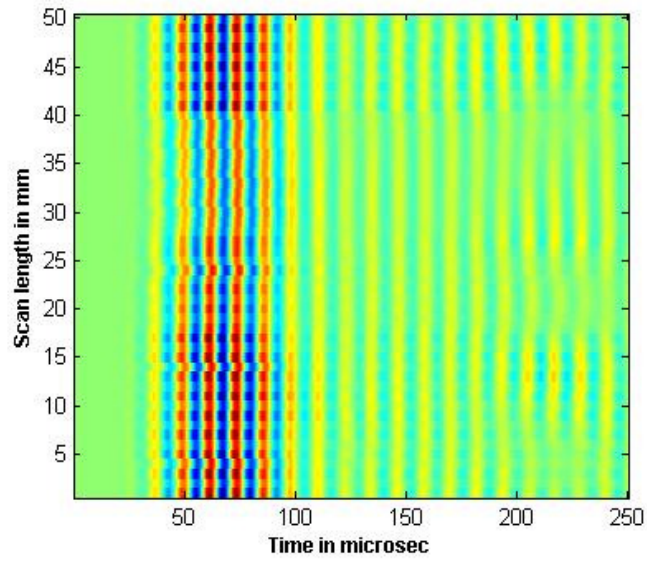


**Fig.16: Numerical B-Scan of marcel AR6 at 100 KHz, and placed at 6mm**

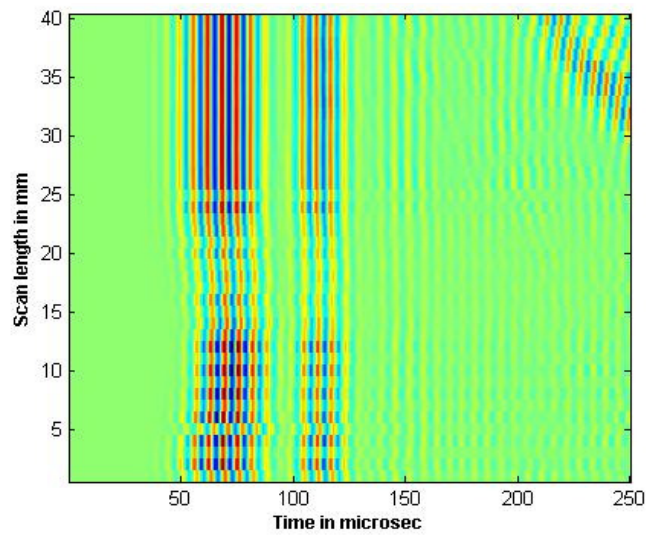


**Fig.17: Numerical B-Scan of marcel AR6 at 200 KHz, at 6mm**



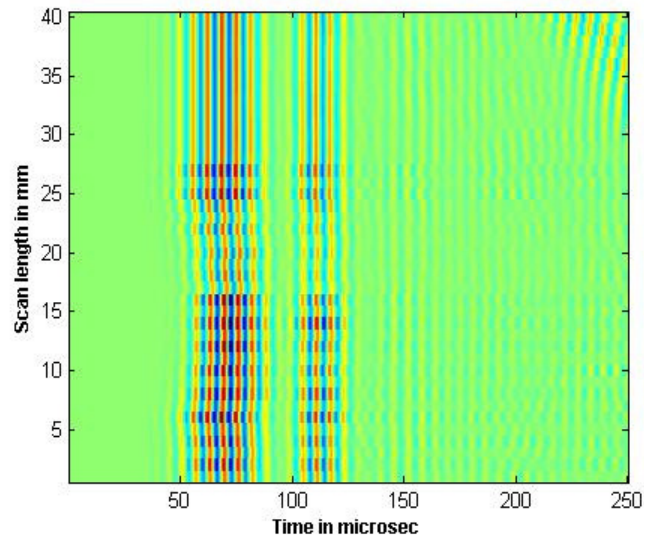


**Fig.18: Numerical B-Scan of marcel AR6, at 12mm**

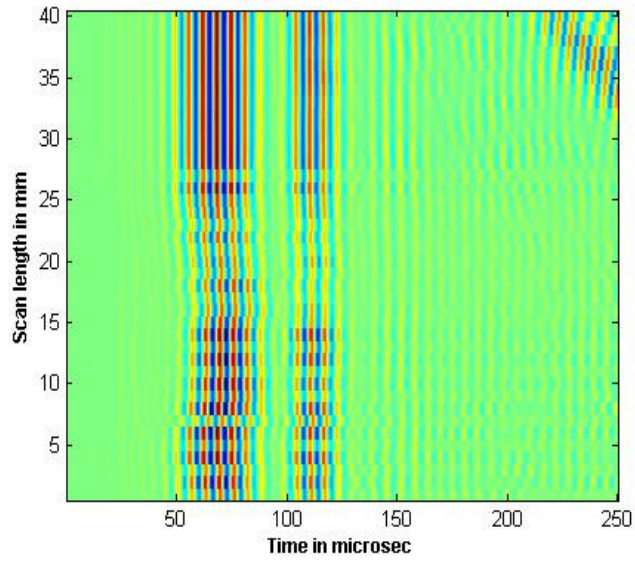


**Fig.19: Numerical B-Scan of marcel AR6 at 18mm**



To study the change in TOF, Hilbert transform was performed on each signal and the peak in each case was isolated to extract the TOF data, and plotted against distance. The plots for 6, 12 and 18mm for a marcel of AR 6 are shown in Figure (20), (21), and (22).

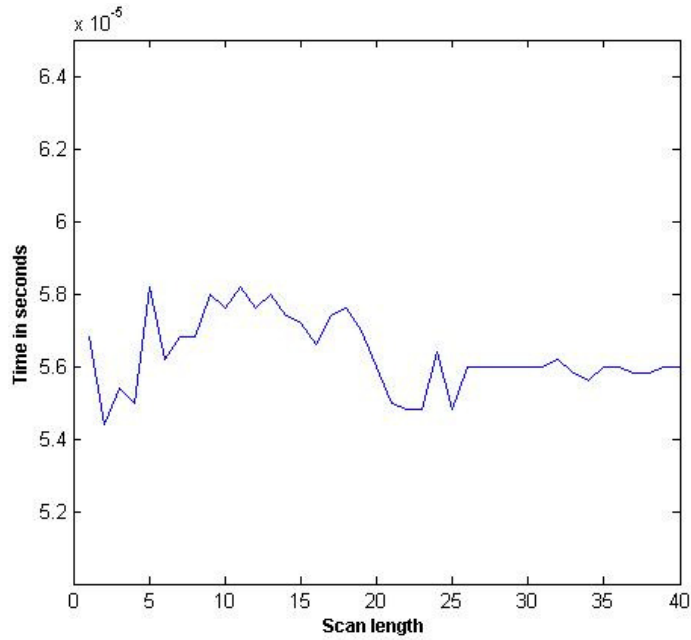


**Fig.20: Hilbert transform of B-Scan for marcel at6mm(Shown in Fig.15)**

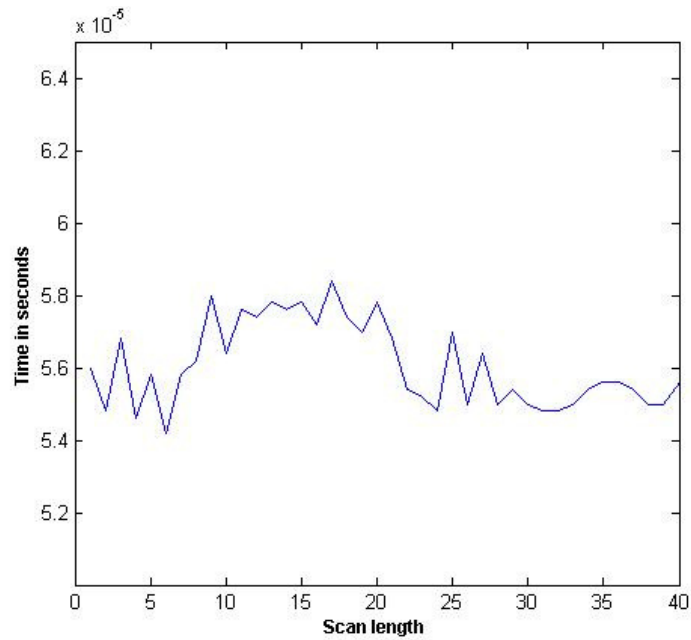


**Fig.21: Hilbert transform of B-Scan for marcel at12mm (Shown in Fig.16)**

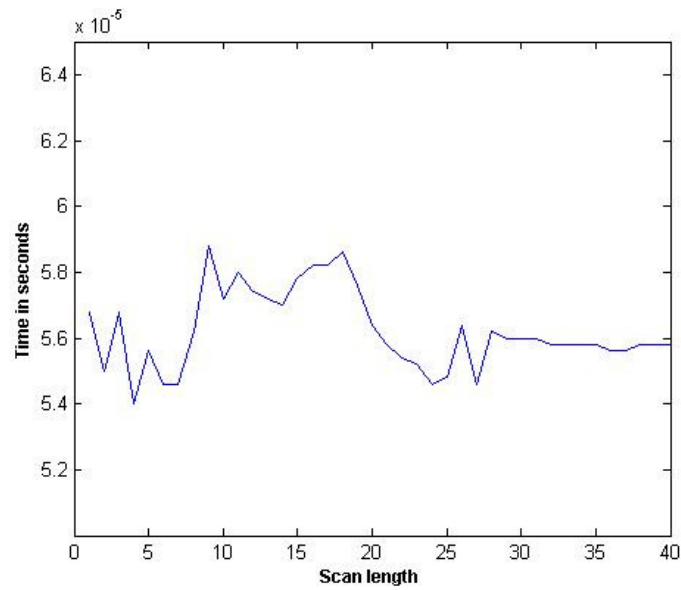


**Fig.22: Hilbert transform of B-Scan for marcel at18mm(Shown in Fig.17)**

Although the TOF change is not appreciable, the initial step of mapping the change of velocity while traversing over the marcel was considered a good initiation point for the finite element study. The same procedure was repeated for AR 10, and AR 14, but no significant change in TOF or amplitude was observed. The lack of sensitivity can be attributed to the mesh size of the model and the computational limitations. In the model each glass fiber layer had only one element in the thickness direction and hence capturing the effect of thickness variation of each layer was difficult. With refined mesh containing at least 2 to 3 elements per layer in the thickness direction, the effect might be captured well. But since such a model would be computationally intensive and time consuming, it is currently incomputable with the available resources.

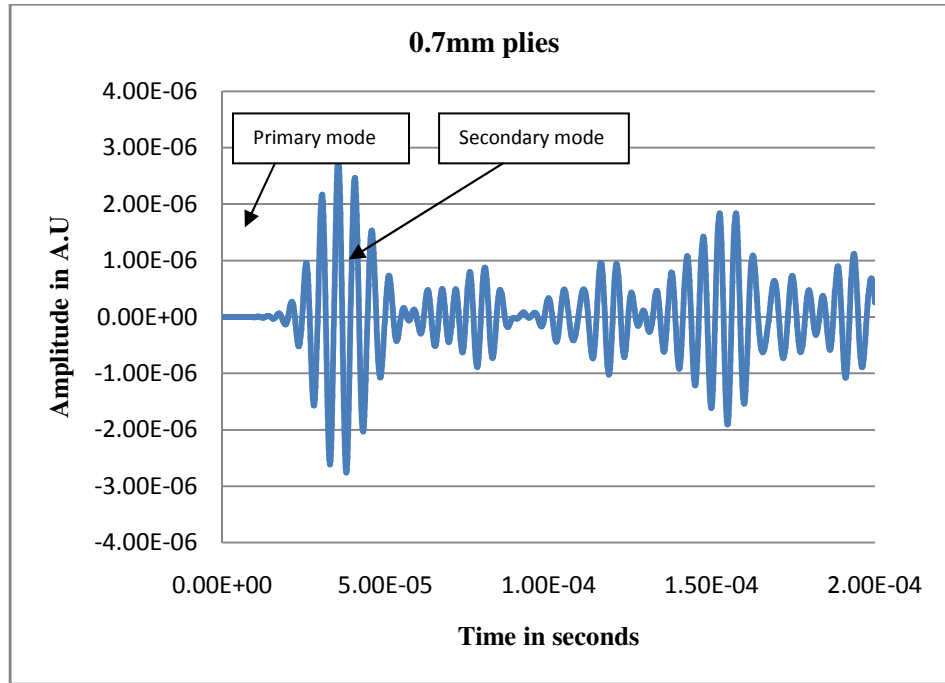


Fig.23: A-Scan of 0.7mm ply laminate (40 layers). The primary and secondary modes are shown.

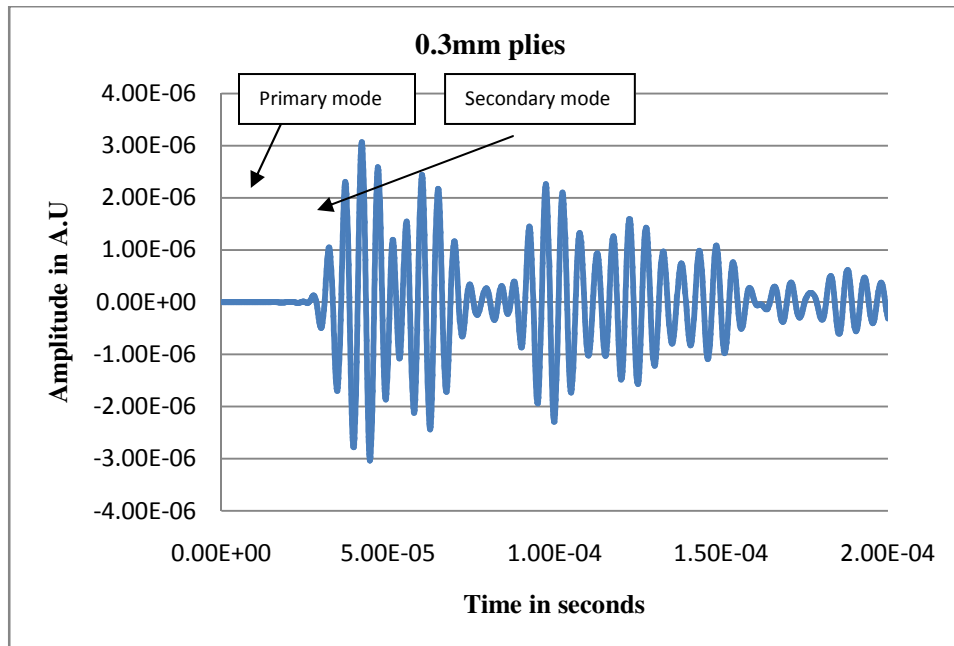


Fig.24: A-Scan of 0.3mm plies laminate (40 layers). Notice the secondary mode travelling faster than the secondary mode of 0.7mm ply.

## 8. DISCUSSIONS

The generation of a secondary mode as seen in Figure (23) and Figure (24) with change in layer thickness, suggests the dispersion effect of Rayleigh wave due to layer anisotropic media. Although the Rayleigh wave equation for isotropic media is devoid of a frequency term, it has to be considered for anisotropic media as shown in Equation (23). The effect of layer anisotropic media was captured well using FEM, and is evident from Figure (23), Figure (24). Velocity measurements of these signal waveforms showed that the secondary mode was faster than the primary mode while traversing over the marcel. This is consistent with both the experimental and numerical B-Scan data shown in Sections 6.3 and 7.1.

The marcel can be defined in terms of geometric distortions, but the change in thickness of the layers has to be compensated elsewhere since the top and bottom surface remain flat. Rayleigh wave propagation in such a scenario will be affected by the variation of thickness of the different layers and the effect can be seen as a change in velocity. Although the change in TOF is only a few microseconds, the change in velocity is significant, which shows the dispersion effect of Rayleigh waves due to thick layered anisotropic media.

The purpose of determining the orientation of the marcel is very significant, since the upward and downward marcel behave differently. A single step, static analysis using FEM, showed that the two marcel act completely different depending on the loading. The results of four point bending test using FEM for the upward and downward pointing marcel are shown in Figure (26) through Figure (29). A schematic of the measurement of stress is shown in Figure (25).

The Y direction stress ( $\sigma_Y$ ) for the downward and upward marcel in Figure (26) and Figure (27), shows a high compression stress developed in the downward marcel at the center of the wave. Beyond the marcel, in the straight fiber region, the shear stress seems to reduce and become zero. A similar pattern is observed for the upward pointing marcel, but the stresses are in tension unlike downward pointing marcel. Figure (28) and Figure (29) show the shear stress ( $\sigma_{XY}$ ) developed in the upward and downward marcel. At the center of the marcel, there is no shear stress developed in the upward marcel, but a considerable amount of stress is developed in downward marcel. This shows the difference in the mechanics between the two marcel despite one being reverse of the other. Although an upward pointing marcel looks more detrimental from Figure (28), the possibility of an upward marcel developing closer to the top surface without out-of-plane surface protrusion is rare. But the downward marcel can easily form close to the surface and can go undetected with traditional methods.

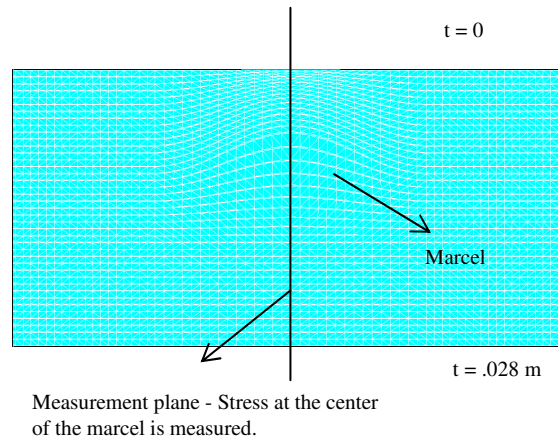


**Fig.25: The measurement plane in the XY plane of the upward marcel.**

We can see that both the upward and downward marcel are detrimental to the structure, but knowing the orientation of the marcel gives us the knowledge of whether it's severe or not.

This highlights the importance of knowing the orientation of the marcel.

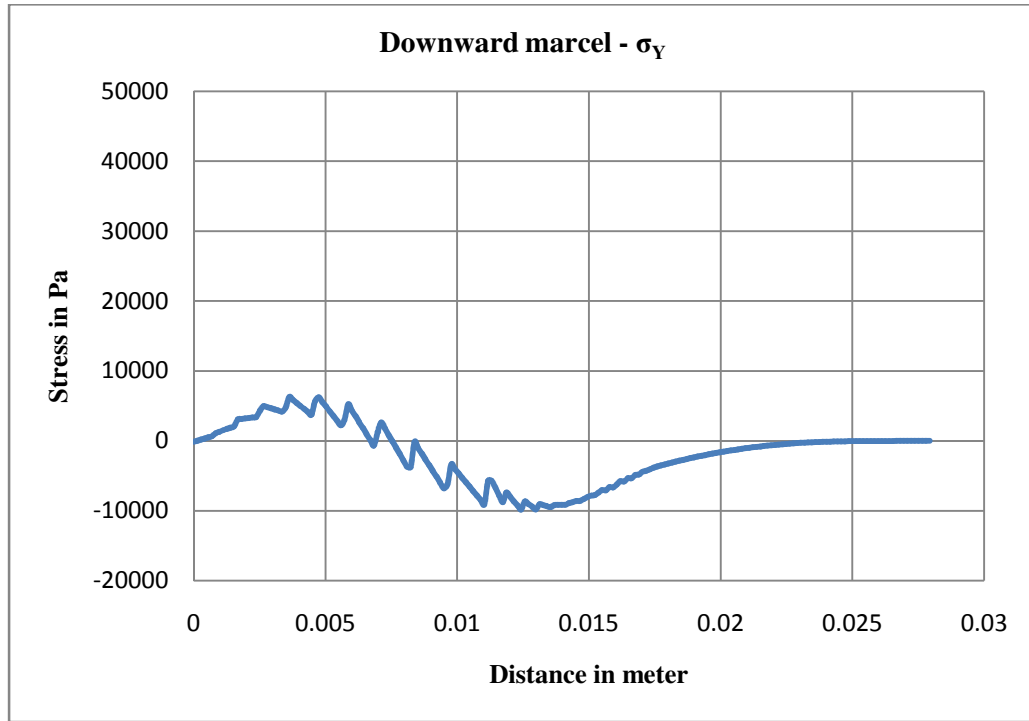


Fig. 26: Out of plane stress (Y) distribution for downward pointing marcel (AR 6) across the thickness at the center of marcel.

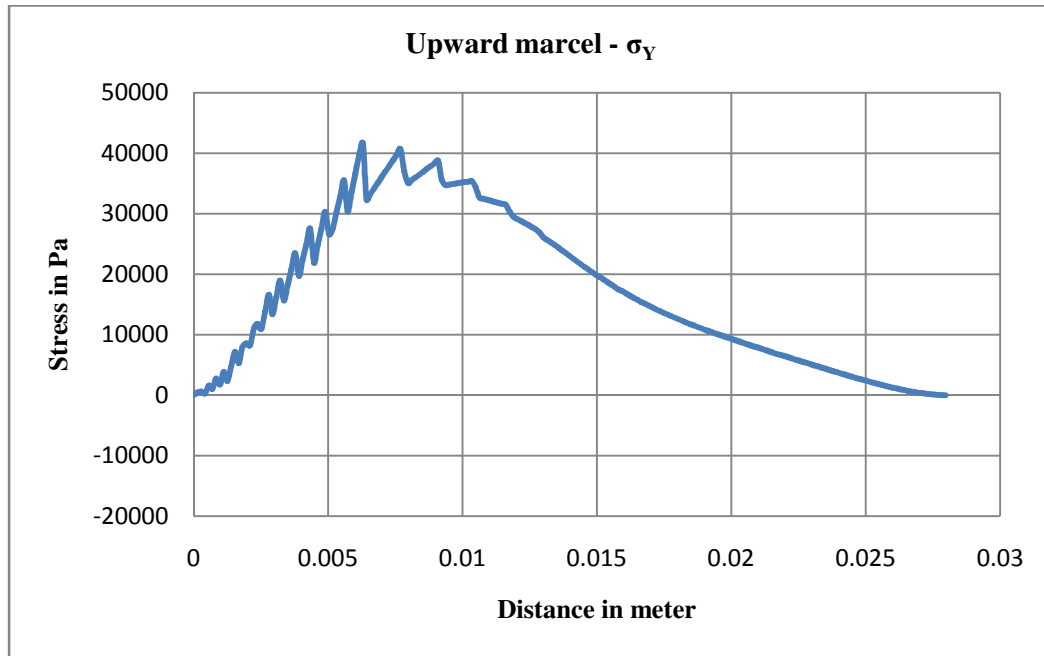


Fig.27: Out of plane stress (Y) distribution for upward pointing marcel (AR 6) across the thickness at the center of marcel.

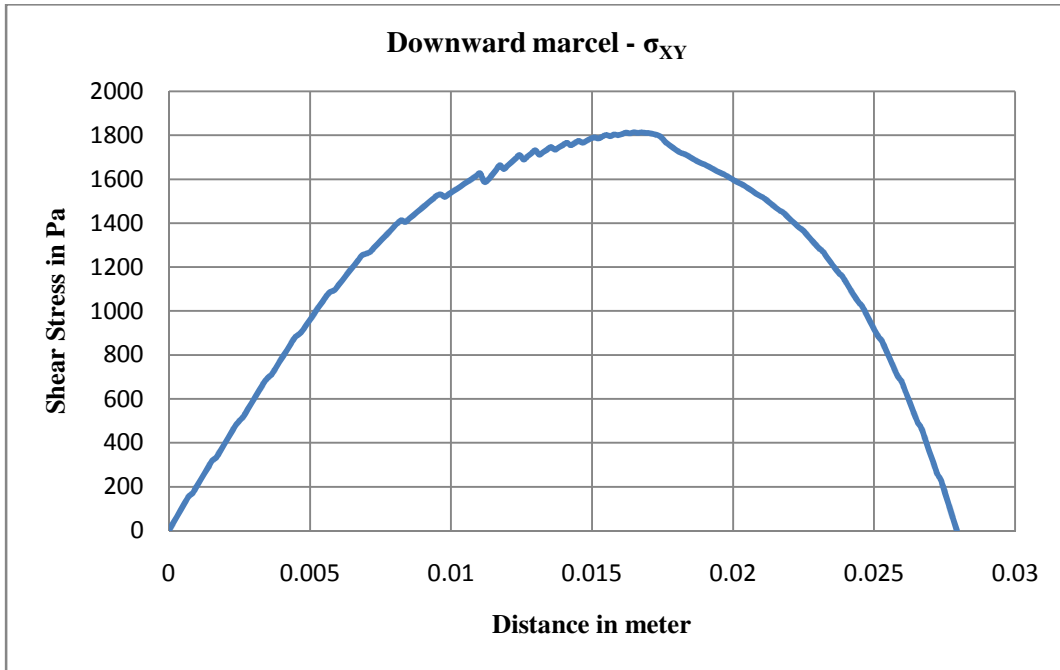


Fig.28: Shear Stress ( $\sigma_{XY}$ ) distribution for downward pointing marcel (AR 6) across the thickness at the center of marcel.

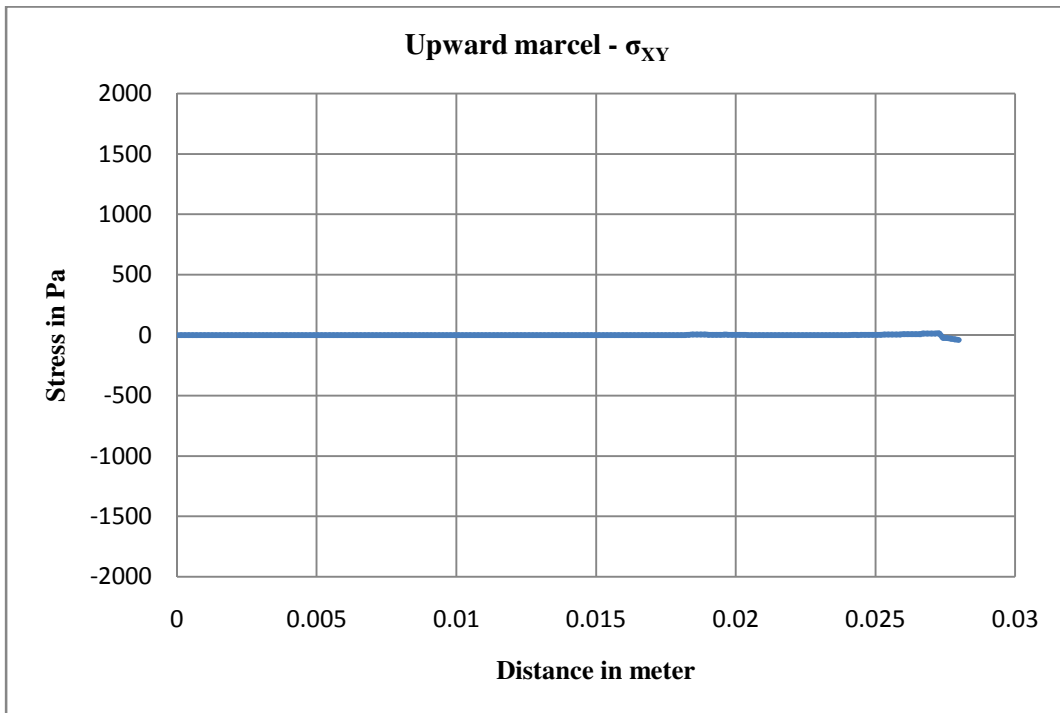


Fig.29: Shear Stress ( $\sigma_{XY}$ ) distribution for upward pointing marcel (AR 6) across the thickness at the center of marcel.



## 9. CONCLUSION

This paper presents the results from the investigation of single sided inspection of composite wind turbine blades for intrinsic, discrete, and out of plane marcel or waviness. The three step approach is believed to hold potential for making a field implementable system, with a higher sensitivity to waviness compared to other methods. By characterizing the marcel with the help of aspect ratio, i.e. geometric changes, changes in velocity, phase shift and amplitude, this method is simple and reliable. The field adaptability of this system, coupled with the cost effectiveness and speed of scanning makes it a highly preferable method for NDE of wind turbine blades. Furthermore a detailed analysis of the effects of dispersion of Rayleigh waves in layered anisotropic media needs to be performed. A fine mesh finite element model with 2-3 elements per layer in the thickness direction will be modeled to confirm the findings. A 3D model which may be able to capture the dispersion effects will be created and studied.

### CHAPTER 3. BOND THICKNESS MEASUREMENT

The wind turbine blade is manufactured as two halves and bonded together using high quality adhesive. The two halves are joined along the edges and in the middle a spar is placed which in turn provides the bending stiffness of the blade. The bond-line extends along the trailing edge, leading edge and the shear web to the lower and upper halves. The shear web and spar cap joint is considered one of vital joints in the structure since together they act as an I beam as shown in Figure (3.1). The inspection of such a joint for lack of adhesive, or thickness of adhesive becomes very important. For this purpose ultrasonics NDE using contact transducers were used. This type of inspection already exists in manufacturing companies, but a field scaled effort in production line is not available. One of the objectives of this research is to design a field implementable bond-line inspection system which can measure the bond-line thickness, perform C –Scans to determine defects such as lack of adhesive, or voids in adhesive. To facilitate this, a scanning method using contact transducers was devised and is explained in the following section.

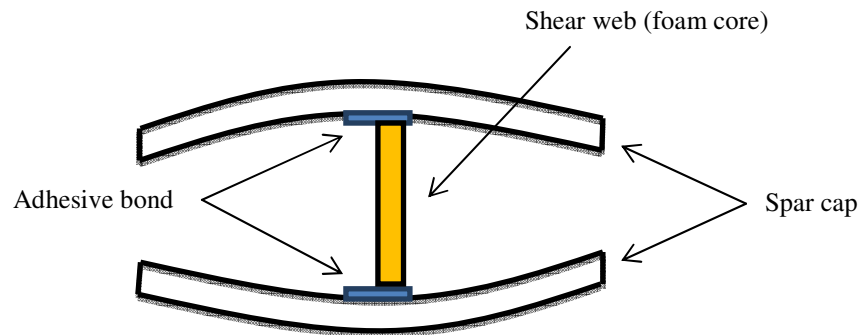
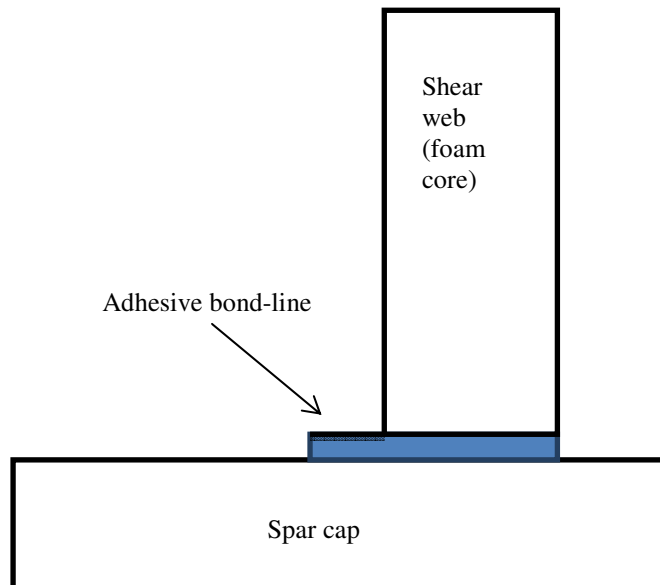


Fig. 3.1: Section of the bond joint between the two halves of the blade.

### 3.1. METHOD AND THEORY

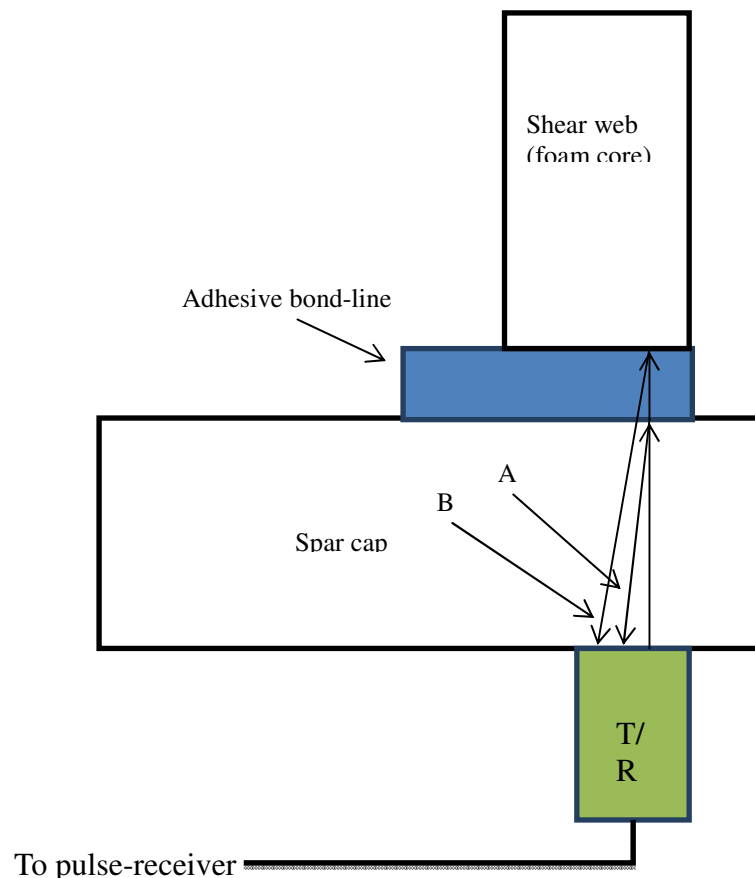
Optimization of frequency was the first step in the methodology. Contact transducers of frequency range from 100 KHz to 2.25 MHz were used to optimize the frequency. At 500 KHz, a strong signal with less attenuation was observed in the spar cap sections. A schematic of the spar cap/shear web bond is shown in Figure (3.2).



**Fig. 3.2: Schematic of shear web/spar cap joint bond-line.**

Pulse echo mode of measurement was used to inspect this joint. By impinging the surface with an ultrasonic wave, stress waves are created in the structure which travel through the thickness of the structure and a portion of it gets reflected at the interface. The reflected signal returns as the echo for the initial pulse (shown as A in Fig. (3.3)). The other portion gets transmitted through the bond-line, and gets reflected at the end of the shear web. This is

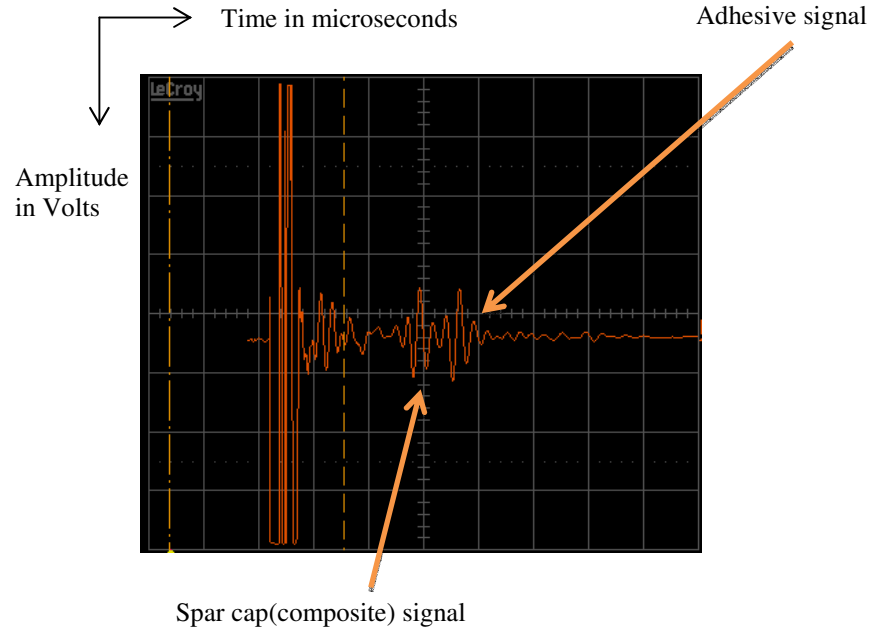
obtained as the second signal in time domain (shown as B in Fig. (3.3)). This is explained schematically in Figure (3.3). By taking the difference in the time of arrival between the two signals we can obtain the time of flight (TOF) in the adhesive region. Knowing the speed of sound in adhesive, we can determine the thickness using TOF. This method has been consistently used for bond-line measurement, but using it for thick composite plates, (spar cap sections of more than 1.5 inches) is the challenge.



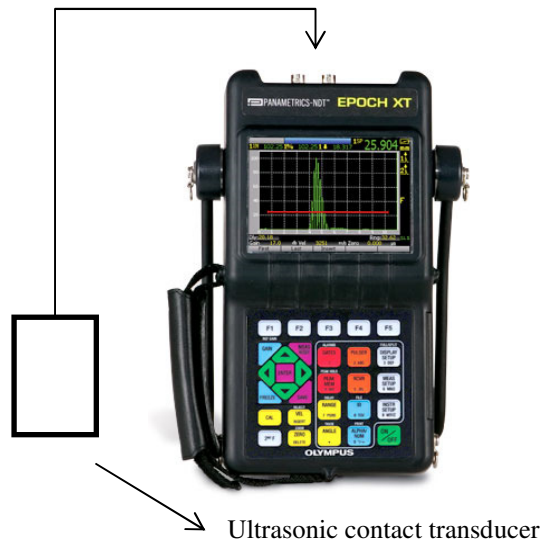
**Fig.3.3: Schematic of pulse echo method used for inspection.**

Figure (3.4) shows the time domain signal from the adhesive and spar cap interfaces as explained in Figure (3.3). The peak to peak difference in time was measured to give the

difference in TOF. The velocity of sound in adhesive was measured by using finely machined cubes of adhesive and repeating pulse echo measurements to obtain the TOF.



**Fig.3.4: The adhesive and spar cap signal in time domain.**



**Fig.3.5: schematic of bond-line measurement setup**

### 3.2 EXPERIMENTAL SETUP

The setup used for measurements is shown in Figure (3.5). The Olympus EPOCH XT was used as a pulse/receiver and display unit for measurement of bond-line. The pulse-receiver was operated at 100 KHz PRF, and 40DB gain. Individual A-Scans could be stored and retrieved, but the online-display of EPOCH XT can also display the thickness directly with the help of measuring GATES, which made the measurements faster. Together the system was portable and field implementable.

### 3.3 RESULTS

Bond thickness measurements were carried out along the length of the blade on the high pressure and low pressure side. Since the spar cap thickness varies along the length of the blade, some measurements were inconsistent and hence were not reported. But an overall variation of bond-line thickness along the length of the blade could be obtained. Point scans measuring the thickness of adhesive at one meter intervals were taken, and the thickness was plotted against the length of the blade. Due to proprietary nature of the collected data, it cannot be published in this thesis. But the method was verified to work in the field.

### **3.4 DISCUSSIONS**

With the help of bond thickness variation along the length of the blade, blade manufactures can optimize the manufacturing process to ensure the correct amount of adhesive is applied between the shells. This method can be extended to a complete scanning system, by using ultrasonic transducers to obtain the adhesive signal in pulse echo mode. The absence of a second signal in time domain denotes the absence of adhesive in the particular region. By performing a C-Scan (spatial location vs. amplitude), we can obtain the spatial locations of the defective regions. In the presence of the second signal, we can use GATES to track the signal and obtain the thickness in the region directly. This system will be field implementable and will be considered for future work.

## **CHAPTER 4. CONCLUSIONS**

### **4.1 SUMMARY**

We have described here the use of ultrasonic non-destructive evaluation to inspect wind turbine blades for defects. The types of defects investigated here include fiber waviness and bond thickness measurement and inspection. A two-step method was developed for waviness investigation, and was used to build a stand-alone inspection system which can be deployed for field inspection. This concept can be extended to build a process NDE system which can be implemented on the production line to eliminate defective blades at production level. The effect of waviness on Rayleigh wave propagation was theoretically confirmed using finite

element models. Numerical modeling was able to capture the change in time of flight (TOF), and the results are consistent with experimental results.

The second type of defect described in this thesis is the bond joint inspection. Pulse-echo mode of ultrasonic measurement was used to measure the thickness of adhesive at the spar cap/shear web joint. This is one of the vital portions of the structure and hence stringent quality control is necessary. By analyzing the time domain data of signal waveform, and using the difference in TOF, the thickness of adhesive was measured. Using a standalone system for measurement, a field implementable method to monitor the variation of bond thickness along the length of the blade was devised. This concept can be extended to build large scale, field implementable scanning system capable of scanning the entire blade.

## **4.2 FUTURE WORK**

A finer mesh 2D finite element model of waviness will be modeled to further understand the effect of waviness on Rayleigh wave propagation. This will help us in the quantification of the marcel's better. The analysis will be extended to 3D model to understand the mechanics of elastic wave propagation in the blades. The multimode generation and velocity change as a result of dispersion effects of Rayleigh waves will also be explored.

A field implementable bond thickness measurement system will also be developed.



## REFERENCES

- [1] Zbigniew Lubosny (2003). *Wind Turbine Operation in Electric Power Systems: Advanced Modeling (Power Systems)*. Berlin: Springer. ISBN 3-540-40340-X.
- [2] Borum K. K, Mc Gugan M. and Brondsted P. Condition monitoring of wind turbine blades. Proceedings of the 27<sup>th</sup> Riso International Symposium on Materials Science: polymer composite materials for wind power turbines. Denmark 2006 P 139-145.
- [3] H.M. Hsiao & I. M. Daniel, "Effects of fiber waviness on stiffness and strength reduction of unidirectional composites under compressive loading", *Composites science and technology*, 1996.
- [4] Chandra S Yerramalli, Thomas Miebach, Karthick Chandraseker and Shu Ching Quek, "Fiber waviness induced strength knockdowns in composite materials used in wind turbine blades", Proceedings of European wind energy conference and exhibition, 2010.
- [5] Gretchen B. Murri, "Influence of ply waviness on fatigue life of tapered composite flexbeam laminates", NASA/TM -1999-209830, ARL-TR-2110.
- [6] Mandell, J.F. Samborsky, D.D., and Wang, L., "Effects of Fiber Waviness on Composites for Wind Turbine Blades," Proceedings of the 48th International SAMPE Symposium, Vol. 48, SAMPE 2003, Long Beach, CA, May 11-15, 2003. pp. 2653 - 2678, ISBN 0-938-99494-8, (2003).
- [7] Daniel O'Hare Adams, Steven Bell, "Compression strength reductions in composite laminates due to multiple-layer waviness", *Composites science and Technology* 53(1995) 207-212
- [8] Castaings M, Cawley P, Farlow R. & Hayward G. "Single sided inspection of composite materials using air coupled ultrasound", *J.Nondestr. Eval.* 1998.17: 37-45.
- [9] V. Dayal, "Wave Propagation in a Composite with a Wavy Sublamina", *Journal of Nondestructive Evaluation*, 14(1), 1995.
- [10] Autar Kaw, "Mechanics of composite materials" second edition, CRC press.
- [11] Stonely, R., "The seismological implications of aeolotropy in continental structure", *Monthly notices Roy. Astron. Soc. Geophysics*, Supp 5, 222-232, 1949.
- [12] Don L. Anderson, "Elastic wave propagation in Layered anisotropic media", *Journal of Geophysical Research*, Volume 66, No.9 September 1961.
- [13] Tadashi Ohyoshi, "The propagation of Rayleigh waves along an obliquely cut surface in a directional fiber-reinforced composite", *Composite Sciences and Technology*, 60 (2000) 2191-2196.
- [14] Shi-Chang Wooh, Isaac Daniel, "Wave propagation in composite materials with fiber waviness", *Ultrasonics*, Vol 33, No 1, page 3-10, 1995.
- [15] Adnan Nayfeh, "Wave propagation in layered anisotropic media with applications to composites", Volume 39, Elsevier publications, 1995.
- [16] Mark Garnich, Ghodrath Karami, "Localized fiber waviness and implications for failure in unidirectional composites", *Journal of Composite materials*, Vol.39, No.14/2005.
- [17] [http://www.designnews.com/article/512395-Sandia\\_Sizes\\_up\\_Wind\\_Turbine\\_Blade\\_Design.php](http://www.designnews.com/article/512395-Sandia_Sizes_up_Wind_Turbine_Blade_Design.php)

## ACKNOWLEDGMENTS

First and foremost, I would like to thank my advisor, Dr. Vinay Dayal, without his insights and teaching methods I would not have been able to finish my thesis. I would also like to thank Dan Barnard for sharing his immense knowledge and technical know-how in experimental ultrasonics, and Dr. David Hsu whose questions on my research work had given me the ability to come up with explanations to the problems myself. I also take this opportunity to thank Andrew Gross, Aaron Eldal, Ryan Krafka, and Steven Green for helping me make the samples needed for experimental work. Special thanks to Arun Chander Kalyanasamy and Sri Ramya Mallipudi for helping me proofread my papers and thesis.

Finally I would like to thank my parents and family, without their support my work would have not been possible.